An animal component free bioprocess to synthesize 3D human matrix scaffolds using mesenchymal stromal cells

Shaianne N. Stein [1,2], Lorena R. Braid [1,2*]

[1]Simon Fraser University, Department of Molecular Biology and Biochemistry, Burnaby, BC, Canada

[2]Simon Fraser University, Centre for Cell Biology, Development and Disease, Burnaby, BC, Canada

*** Correspondence:**
Lorena R. Braid
lrbraid@sfu.ca

Keywords: Mesenchymal stromal cells (MSC), spheroid, decellularized matrix, extracellular matrix, collagen, basement membrane, animal component-free

Abstract

Basement membrane is a specialized extracellular matrix (ECM) that compartmentalizes epithelial and endothelial tissues and provides essential structural and signaling cues for tissue organization. While fibrillar collagens (Col) of the interstitial matrix (e.g., Col I and Col III) are widely used in tissue modeling, the networking collagens that scaffold basement membrane, including human Col IV and Col VI, remain difficult to access. Commercial basement membrane surrogates such as Matrigel® are derived from murine tumors and are ill-defined, dilute, variable, and incompatible with animal-free biomanufacturing. Thus, there is a critical need for human-derived basement membrane matrices that are free of xenogenic contaminants and do not rely on animal agriculture.

Here, we investigated whether human mesenchymal stromal cells (MSCs) could serve as a platform to produce self-assembling basement membrane components under chemically defined, xeno-free conditions. MSCs from placental, umbilical cord, bone marrow, and adipose tissues were cultured as three-dimensional spheroids and adherent multilayered sheets. Confocal imaging of whole-mount, decellularized spheroid matrices revealed complex networks of fibronectin and Col IV with topological

and organizational features characteristic of native basement membrane. Perinatal MSCs produced distinct matrix architectures consisting of apical fibronectin sheets underlaid by continuous Col IV networks. Time-resolved imaging of umbilical cord MSC–derived matrix sheets demonstrated a reproducible sequence of basement membrane assembly that parallels developmental tissue organization.

Together, these findings demonstrate that human MSCs, cultured entirely without animal-derived components, can synthesize functional basement membrane proteins that self-assemble into ordered, tissue-like scaffolds. This work establishes MSCs as a scalable, sustainable, and cruelty-free platform for the manufacturing of human basement membrane matrices for bioengineering and regenerative medicine applications.

1 Introduction

The extracellular matrix (ECM) plays a central role in tissue organization, morphogenesis, and cell fate determination, making it a critical component of bioengineered human tissues and organoid systems (Jain et al., 2022; Kozlowski et al., 2021; Motta et al., 2023; Olesen et al., 2021). While interstitial matrix provides essential structural support, tensile strength, and scaffolding for cells within connective tissues, basement membrane–type matrices provide essential biochemical and structural cues that regulate epithelial and endothelial polarity, vascularization, and growth factor signaling (Jain et al., 2022; Jayadev & Sherwood, 2017; Khalilgharibi & Mao, 2021; Pompili et al., 2021; Sekiguchi & Yamada, 2018; Yurchenco, 2011). Despite their importance, the development of human-relevant basement membrane scaffolds remains limited by the availability of appropriate matrix materials (Aisenbrey & Murphy, 2020; Perugini & Santin, 2021).

45 Currently, basement membrane surrogates such as Matrigel® and Cultrex™ are widely used in three-
46 dimensional (3D) culture systems (Aisenbrey & Murphy, 2020; Kane et al., 2018). However, these
47 materials are derived from murine Engelbreth–Holm–Swarm sarcoma and only distantly resemble
48 native human basement membrane in composition and organization (Huang et al., 2021; Hughes et al.,
49 2010; Kleinman & Martin, 2005; Kozlowski et al., 2021). Their reliance on animal agriculture raises
50 ethical and sustainability concerns, while xenogeneic contaminants, batch-to-batch variability, and
51 undefined bioactive components limit experimental reproducibility and translational applicability
52 (Aisenbrey & Murphy, 2020; Baker, 2016a, 2016b; Hemeda et al., 2014; Jung et al., 2010; Liu et al.,
53 2023). Given the harsh conditions required to solubilize tumor matrix proteins, these hydrogels likely
54 contain fragmented ECM proteins that are incapable of physiologic matrix self-assembly (Hughes et
55 al., 2010; Tuftee et al., 2024).

56 Human cell–derived ECM represents a promising alternative, as cells can synthesize, process, and
57 assemble matrix proteins into organized networks that more closely resemble native tissue architecture
58 (Fonseca et al., 2023; Franco-Barraza et al., 2016; Muiznieks & Keeley, 2013; Solomonov et al., 2025).
59 Approaches including tissue decellularization and cell-generated microtissues have demonstrated the
60 feasibility of producing human ECM scaffolds *in vitro* (Chen et al., 2025; Chiang et al., 2021; Duisit
61 et al., 2018; Fonseca et al., 2023; Jin et al., 2022; Johnson et al., 2016; Malakpour-Permlid et al., 2021;
62 Zhang et al., 2023). Mesenchymal stromal cells (MSCs) are attractive candidates for matrix production
63 due to their availability from multiple tissues, robust secretory capacity, and established use in
64 biomanufacturing (Fonseca et al., 2023; Pompili et al., 2021; Smith et al., 2020; Tao et al., 2020).
65 However, most studies of MSC-derived ECM have relied on animal-derived supplements such as fetal
66 bovine serum (FBS) or human platelet lysate (hPL) (Amable et al., 2014; Chen et al., 2025; Maia et
67 al., 2014; Novoseletskaya et al., 2020; Sagaradze et al., 2020; Yin et al., 2024).

68 The use of serum-based culture systems presents significant limitations for matrix manufacturing.
69 Growth factors present in FBS and hPL become sequestered within the ECM, embedding xenogeneic
70 or donor-dependent proteins that compromise matrix definition, reproducibility, and downstream
71 applications (Baker, 2016a, 2016b; Hemeda et al., 2014; Jung et al., 2010; Keppie et al., 2021; Liu et
72 al., 2023; Zhang et al., 2017). Chemically defined media offer a path toward reproducible, animal-
73 component-free bioprocessing (Malakpour-Permlid et al., 2025; Oredsson et al., 2025; Weber et al.,
74 2024), but these formulations lack the complex growth factor milieu found in serum and are often
75 associated with reduced cellular performance (Hemeda et al., 2014; Jung et al., 2010; Spoerer et al.,
76 2025; Xu et al., 2020). Critically, matrix production requires not only synthesis of ECM proteins, but
77 also coordinated expression of processing enzymes necessary to convert precursor molecules, such as
78 procollagens, into mature, self-assembling networks (Muiznieks & Keeley, 2013; Solomonov et al.,
79 2025). Whether chemically defined media can support this level of MSC-mediated matrix assembly
80 remains unknown.

81 Here, we investigate whether human MSCs from multiple tissue sources can self-assemble basement
82 membrane–type matrices under fully defined, animal-component-free conditions. Using a quality-by-
83 design approach compatible with GMP manufacturing, we show that MSCs cultured in chemically
84 defined media form three-dimensional spheroids and adherent multilayered sheets that deposit Col IV–
85 positive basement membrane matrices. These matrices contain canonical basement membrane
86 components, can be decellularized, and support recellularization, demonstrating their potential as
87 scalable and human-relevant ECM scaffolds for bioengineering applications.

88 **2 Materials and Methods**

89 2.1 Cell source

90 High quality human MSCs were obtained from commercial sources. UC were provided by Tissue
91 Regeneration Therapeutics (TRT), Inc. (Toronto, Canada). UC MSCs were isolated from the
92 perivascular Wharton's jelly of healthy term (>37 weeks) umbilical cords from 1 male infant delivered
93 by C-section and cryopreserved at mean population doubling level (mPDL) 4.87. AD and BM MSCs
94 from female donors were obtained from RoosterBio Inc. (Frederick, MD) at 8.9 and 8.8 mPDL,
95 respectively. PL MSCs from a female donor was obtained from OrganaBio (Miami, FL) at mPDL 8.39.
96 Experiments were performed using one donor population per tissue of origin. For whole mount
97 immunostained spheroids (Section 2.7), 3 UC MSC donor populations were pooled and cultivated.

98 2.2 Cell culture and maintenance

99 For cell expansion, MSCs were seeded at a density of 1,333 cells (UC MSCs) and 3,000 cells (AD,
100 BM, PL MSCs)/cm^2 in chemically defined phenol red-free MSC NutriStem XF® complete growth
101 media (Sartorius AG, USA). Cells were seeded according to TRT and RoosterBio's recommended
102 seeding density and expansion protocols which have been optimized for maximal cell expansion.
103 Culture-ware was pretreated with 2.67µg/cm^2 Col IV from human placenta (MilliporeSigma) to
104 facilitate adherence. Cells were maintained in physioxia at 37°C, 5% CO_2, 5% O_2 and 80% relative
105 humidity in a Heracell VIOS 160i tri-gas incubator (ThermoFisher Scientific, Waltham, MA). At 70-
106 80% confluence, MSCs were washed briefly with Dulbecco's phosphate buffered saline (DPBS;
107 MilliporeSigma) and enzymatically detached by 2-3 minute incubation with TrypLE Select
108 (ThermoFisher Scientific, Waltham, MA). Upon complete dissociation, an equal volume of media was
109 added to the cell suspension and cells enumerated using the CellDrop Fluorescent Cell Counter
110 (DeNovix Inc., USA). Cells were pelleted by centrifugation at 150 x *g* for 5 minutes and the cell pellet
111 resuspended in fresh chemically defined media before re-seeding. All experiments were performed
112 using MSCs between PDLs 16-24.

113 2.3 Self-assembled spheroids

114 Spheroids were generated using a protocol adapted from Li et al (Li et al., 2021): 96-well plates were
115 coated with 75µl of sterile 1% agarose (w/v) and allowed to solidify at room temperature. Coated
116 plates were used immediately or stored up to 1 week in 80µl DPBS per well. DPBS was aspirated prior
117 to seeding. MSCs were suspended in NutriStem XF® culture media at a concentration of 437,500
118 cells/ml (35,000 cells/well). 80µl of cell suspension was added to the coated wells and spheroids were
119 allowed to spontaneously aggregate over 4 days in the incubator. To generate spheroids of different
120 sizes, UC MSCs were cultivated using initial cell counts of 7,000, 15,000, 35,000, or 75,000 MSCs per
121 well.

122 2.4 Morphometric analysis

123

124 To quantify differences in spheroid morphology across MSC tissue sources, AD, BM, PL and UC
125 MSCs spheroids were nucleated using 35,000 cells/well. Phase contrast images were captured on days
126 1, 2 and 4 using an Echo Revolve inverted microscope (ECHO Inc., USA) with 10X objective for
127 morphometric analysis. Images were acquired on days 1, 2 and 4 and processed using Adobe Photoshop
128 2023 (24.0.1, Adobe, USA). Spheroids were selected using Object Selection. In cases where the
129 background was too high for auto-selection, the Magnetic Lasso tool was used to manually trace the
130 spheroid perimeter. The background was replaced with grey as a separate layer using Photoshop to
131 restrict calculations of each spheroid. For the initial spheroid seeding density experiments, the Ruler
132 tool was used to measure spheroid diameter after 4 days in culture. Next, the Measure tool was used to
133 automatically quantify spheroid area, perimeter and circularity. At least 19 spheroids per biological
134 replicate, per tissue source were quantified.

135 2.5 Multilayered MSC sheets

136 MSCs were expanded and maintained to harvest an appropriate number of cells for experiments. High-
137 density MSCs (7,813 cells/cm^2) were seeded into 24 well plates in chemically defined media with
138 media changes every 2-3 days and incubated at 37°C, 5% CO_2, 5% O_2 and 80% relative humidity. At
139 specified timepoints (days 1, 2, 4 or 7 after seeding), MSCs were washed with DPBS and then
140 decellularized (see section 2.6) for subsequent immunostaining.

141 2.6 Decellularization

142 Spheroids and multilayered sheets were washed twice in 1X DPBS for 5 minutes each then incubated
143 in decellularization solution (20mM NH_4OH + 0.5% Triton-X100 plus 1X cOmplete^{TM} EDTA-free
144 protease inhibitor cocktail (Roche)) for 30 minutes at 37°C, 5% CO_2, 5% O_2 and 80% relative humidity.
145 To remove residual DNA, the decellularized spheroids were washed twice more in DPBS, then treated
146 with 50kU of DNAse I plus EDTA-free protease inhibitor diluted in water for 30 minutes at 37°C, 5%
147 CO_2, 5% O_2 and 80% relative humidity. The washes were repeated and then the spheroids were stored
148 at 4°C for whole mount immunofluorescence or submerged in 75µl radioimmunoprecipitation (RIPA)
149 buffer and immediately flash frozen in liquid nitrogen and stored at -80°C until use for western blot
150 analysis.

151 To assess retention of cellular material after decellularization, untreated MSC sheets were
152 immunostained with anti-carboxymethyl lysine (anti-CML; 1:200; ab125145; Abcam, USA) as
153 detailed in Section 2.7. The sheets were imaged, then decellularized and re-imaged (Fig S1A). All
154 images were captured using a Nikon ECLIPSE Ti2-E inverted microscope with the 20X objective lens.

155 Retention of nuclear material after decellularization was assessed using FIJI analysis of DAPI-stained
156 decellularized matrices (Fig S1.B). DAPI 16-bit images were imported and threshold with black
157 background was set for the cellularized (913-65535) and decellularized (1600 or 2724- 65535)
158 respectively. A gaussian blur with sigma factor 2 was applied with auto thresholding set to "default

159 dark". The images were masked based on the thresholding values, and the "analyze particles" tool was
160 used to obtain nuclei count. Intact nuclei were counted from at least 10 fields of view for each of 3
161 decellularized wells and 1 cellularized well in each experiment (Fig. S1C). Decellularization efficiency
162 was calculated as the percent of nuclei in decellularized wells compared to cellularized wells.

163 2.7 Immunofluorescence

164 Spheroids and sheets were immunostained in 1.5ml microcentrifuge tubes with nutation or in-well,
165 respectively. For confocal imaging, UC MSCs were seeded at 4000 cells/cm^2 onto coated IBIDI 8-well
166 chamber slides. Cellularized samples were fixed in 10% neutral buffered formalin (NBF;
167 MilliporeSigma) for 10 minutes, rinsed in 1X DPBS and then permeabilized with PBT (1X DPBS +
168 0.1% TritonX-100) for 10 minutes. Following 3 washes in 1X DPBS, samples were blocked with 10%
169 normal donkey serum (MilliporeSigma) diluted in PBST (PBS + 0.1% Tween-20) for 30 minutes.
170 Primary antibodies against human collagen IV (Col IV, 1:200, NovusBio NB120-6586; Col IV alpha
171 1 NC1, 1:100 Chondrex 7070), laminin (LM, 1:200, NovusBio NB300-144), fibronectin (FN, 1:200,
172 NovusBio AF1918) collagen VI alpha 1 (Col VI, 1:200, NovusBio NB120-6588) or lysl oxidase-like
173 2 (LOXL2, 1:100, Abnova 675-773) were diluted in antibody dilution buffer (PBS + 0.1% Triton-X100
174 with 1% bovine serum albumin (BSA)) (MilliporeSigma) and incubated with the sample overnight at
175 4°C. Scaffolds were washed 3 times for 5 minutes each with 1X DPBS at room temperature, then
176 incubated for 1 hour at room temperature with secondary antibodies (donkey anti-Rabbit IgG (H+L)
177 conjugated to AlexaFluor™ 647 (1:1000, Invitrogen A32795), (goat anti-Rat 1gG (H+L) conjugated
178 to Dylight™ 680 (1:500, Novus NBP2-68483FR)) or donkey anti-Sheep IgG conjugated to
179 AlexaFluor™ 594 (1:1000,Invitrogen A110106)) in antibody dilution buffer. The samples were rinsed
180 twice with 1X DPBS and then stained with 4',6-diamidino-2-phenylindole (DAPI, 1:4000,
181 MilliporeSigma) for 2 minutes at room temperature, followed by three 5 minutes each in 1X DPBS.

182 Spheroid samples were stored in Invitrogen Cytovista 3D tissue clearing reagent (ThermoFisher
183 Scientific, Waltham, MA) until mounting. These methods necessitated the use of common animal-
184 derived antibodies and blocking solutions; where possible, we are working to use alternatives like
185 human serum albumin going forward.

186

187 Whole mount imaging of spheroids was facilitated using platform-type slides to accommodate the
188 sample depth and prevent deformation under coverslip pressure. No.2 coverslips were adhered to either
189 end of the microscope slide using clear nail polish to create elevated platforms. The immunostained
190 samples, suspended in Cytovista solution, were pipetted onto the slide and overlaid with a 22x40mm
191 No. 1 coverslip. Mounted slides were sealed with clear nail polish and allowed to set overnight before
192 imaging. Confocal images were captured using a Nikon A1R confocal microscope equipped with
193 PlanFluor 10X DIC L N1 and 40X Oil DIC H N2 lenses. Images were analyzed using NIS Elements
194 software (Nikon Instruments, Inc., USA).

195 Epifluorescent images of matrix deposition in adherent sheets were captured using a Nikon ECLIPSE
196 Ti2-E inverted microscope with the 20X objective lens with 32X averaging on NIS Elements software
197 (Nikon Instruments, Inc., USA). Images were edited using FIJI (v1.54k; (Schindelin et al., 2012)).
198 Wells corresponding to days 1 and 2 were edited to remove background and visualize weak signal.
199 Raw images were imported into FIJI as 16-bit, greyscale images and the brightness and contrast of
200 each image optimized: FN minimum and maximum levels were set to 185 and 400, respectively; Col
201 IV minimum and maximum levels were set to 170 and 600, respectively; Col VI minimum and
202 maximum levels were set to 120 and 275, respectively; LM minimum and maximum levels were set to
203 115 and 540, respectively. Images taken on days 4 and 7 were comparably adjusted to maintain
204 consistency between timepoints. FN minimum and maximum levels were set to 160 and 250,

205 respectively; Col IV minimum and maximum levels were set to 145 and 275, respectively; Col VI
206 minimum and maximum levels were set to 125 and 200, respectively; LM minimum and maximum
207 levels were set to 115 and 190, respectively.

208 2.8 Western blot

209 Total protein was collected from at least 15 pooled, decellularized and DNAse I-treated spheroids per
210 tissue source and replicate. 3D matrices were solubilized by 3 rounds of sonication at 10% amplitude
211 for 30 seconds (1 second on, 1 off). Protein concentration was determined using Bicinchoninic acid
212 assay (BCA; MilliporeSigma) for protein normalization. Samples were diluted and prepared in 6X
213 Laemmli buffer to load 3ug of total protein in 10µl per lane then boiled at 95°C before loading on an
214 8% gel (or 12% for elastin). Proteins were subjected to electrophoresis for 1.5 hours at 140V. Size
215 fractionated proteins were transferred to a nitrocellulose membrane overnight at 4°C at 30V.
216 Membranes were washed three times in 1X Tris Buffered Saline (TBS) for 10 minutes each and then
217 blocked for 1 hour at room temperature in 5% skim milk, or 5% BSA for elastin. The membranes were
218 then incubated with primary antibody solution (rabbit anti-human col IV (1:1000, NovusBio, NB120-
219 6586), rabbit anti-laminin (1:1000, NovusBio, NB300-144), rabbit anti-col VI alpha 1 (1:2000,
220 NovusBio NB120-6588), sheep anti-fibronectin (1:3000, NovusBio AF1918) or rabbit anti-elastin
221 (1:3000, Invitrogen PA5-99418) overnight at 4°C.
222 Membranes were then washed three times in 1X TBST for 10 minutes each. Secondary antibodies
223 (goat anti-rabbit IgG, H+L chain specific peroxidase conjugate (1:3000, Millipore Sigma 401393),
224 rabbit anti-sheep IgG (H+L) secondary antibody (1:4000, Invitrogen 61-8620) or AMDEX™ goat anti-
225 rabbit horseradish peroxidase conjugate (1:3000, Cytiva RPN4301) were diluted in blocking solution
226 and added to the membrane for 1 hour at room temperature. Membranes were washed four times in 1X

227 TBST and visualized using UltraScence Pico Ultra Western Substrate (FroggaBio). Western blots were
228 imaged using an Amersham^{TM} AI600 Imager (GE HealthCare Technologies, USA).

229 2.9 Recellularization of matrix sheets

230 Recellularization of decellularized matrix sheets was assessed using a sample of pooled UC MSCs
231 from 3 donors. Cultured MSCs in T25 tissue culture flasks were pre-stained with Calcein-Green AM
232 (1:1000; ThermoFisher Scientific, Waltham, MA) for 10 minutes, rinsed with 1X Hanks' Balanced
233 Salt Solution with Ca^{2+} and Mg^{2+}, dissociated using 1X TrypLE and centrifuged as described in Section
234 2.2. Calcein-Green labeled MSCs were resuspended at a concentration of approximately 3900 cells/ml
235 in culture media. Unfixed MSC-derived sheet matrices were pre-labeled using anti-FN antibody as
236 described in Section 2.7. Cell suspension was added at a volume of 500 µl/well for 24 well plates and
237 250 µl/well for 48 well plates and incubated overnight as described in Section 2.2. The next day, the
238 culture vessels were placed in a temperature- and humidity-controlled stage top incubator (TOKAI
239 HIT, Co., Ltd., Japan). Time lapse images of cell-matrix interactions were captured every 5 seconds
240 over a 2-minute period using the Nikon ECLIPSE Ti2-E inverted microscope (Nikon Instruments, Inc.,
241 USA) under a 20X objective.

242 2.10 Statistical analyses

243 Statistical analysis was carried out using Prism 10.3.1 (GraphPad Software, LLC). Significant
244 differences were calculated using student's t-test (decellularization efficiency), 2-way analysis of
245 variance (spheroid morphometrics) and Kruskal-Wallis test (spheroid initial seeding density). Error
246 bars represent standard deviation (SD) ± of the calculated means. ns = non-significant, $P>0.05$, * $P \leq$
247 0.05, ** $P \leq 0.01$, *** $P \leq 0.001$ and **** $P \leq 0.0001$. All experiments were performed 3 independent

248 times, exception immunostaining of whole mount spheroid scaffolds which was performed using 2-3
249 technical replicates.

250 **3 Results**

251 3.1 *MSCs from different human tissues self-assemble into 3D spheroids in chemically defined media*

252 We first asked whether MSCs from adult (AD, BM) and perinatal (PL, UC) tissues could reliably form
253 spheroids with an organized matrix in animal component-free, chemically defined conditions. Within
254 four days of high-density seeding on agarose-coated 96-well plates, MSCs from both adult and
255 perinatal tissues formed a single free-floating spheroid in each well (Fig. 1A). A small number of
256 unincorporated cells remained in solution and formed micro-aggregates or attached to the wall of the
257 well, particularly in AD MSC cultures (not shown).

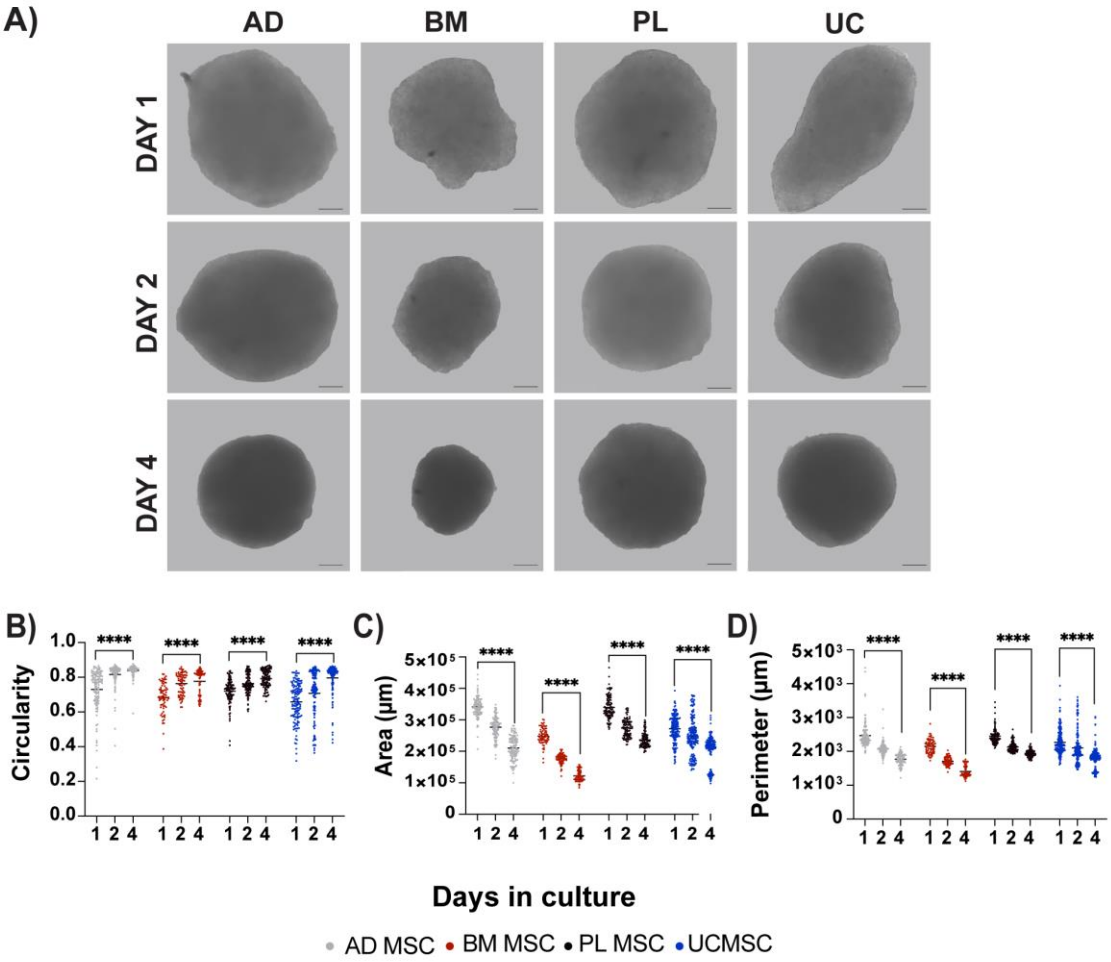

Figure 1: Scaffold-free MSC spheroids exhibit features of self-directed organization. Morphometric analysis of self-assembled MSC spheroids in defined media reveals (A) a visible increase in uniformity which can be quantified by (B) increased circularity (1.0 is a perfect circle), (C) reduced area and (D) decreased perimeter, which together are hallmarks of tissue compaction. Scale bar = 100µm. **** $p < 0.0001$.

Spheroid geometry influences ECM synthesis and organization both directly (Gonzalez-Fernandez et al., 2022) and indirectly by signaling pathways associated with nutrient and oxygen transport (Kumar et al., 2018; Murphy et al., 2017; Shearier et al., 2016), cell–cell interactions (Im et al., 2021) and

267 cytoskeletal tension (Zhou et al., 2017). Accordingly, we quantified spheroid morphometrics
268 (diameter, area, and circularity) over time to assess whether changes in matrix content are associated
269 with, or potentially driven by, alterations in spheroid structure.

270 Over time, the spheroids became increasingly uniform in size and morphology. Circularity (where 1.0
271 is a perfect circle) increased from Day 1 to Day 4 by 11-15% for each MSC type, resulting in average
272 circularities of 0.84, 0.78, 0.80 and 0.80 by Day 4 for AD, BM, PL and UC MSCs, respectively (Fig.
273 1B). Circularity was accompanied by compaction, evidenced by a significant decrease in area (Fig. 1C)
274 and perimeter (Fig. 1D). Spheroids that were much smaller or larger than the mean on Day 1, which
275 may not have aggregated as efficiently or in which there were cell dispensing errors, remained outliers
276 over the time course although their morphometric changes followed the other spheroids.

277 Thus, we next investigated how initial cell density might influence spheroid self-assembly. Spheroids
278 were nucleated using 7,000, 15,000, 35,000, and 75,000 MSCs per well (Fig. 2A). Irrespective of
279 seeding density, all spheroids successfully self-aggregated. Spheroid size increased relative to seeding
280 density, but not linearly (Fig. 2B). All spheroids were visible by eye with diameters ranging from 326
281 to 707µm (Fig. 2A). Excluding the largest aggregates nucleated with 75,000 MSCs, spheroids could
282 be aspirated using a P1000 pipette without shearing. On the other hand, the smallest spheroids were
283 challenging to visualize and manipulate. Considering these practical limitations, as well as reported
284 oxygen diffusion limits (Murphy et al., 2017), we selected spheroids nucleated using 35,000 MSCs and
285 cultured to Day 4 for the remainder of the study.

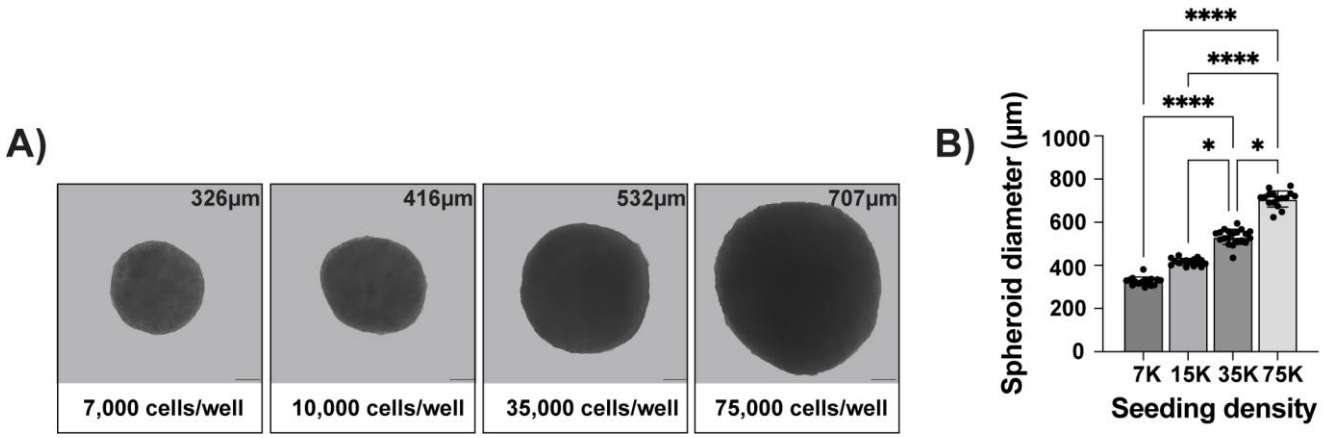

Figure 2: Spheroid diameter correlates with seeding density. Spheroids were seeded in defined media using 7,000, 15,000, 35,000 or 75,000 UC MSCs and measured after 4 days. (A, B) Spheroid size correlated with seeding density, but not in a linear fashion. Average spheroid diameter (µm) (A, upper right corner) was calculated from (B) 15 spheroids per group. Spheroid size was highly consistent between replicates. Representative images are from n=3 independent experiments. Scale bar = 100µm. * $p < 0.5$, **** $p < 0.0001$.

3.2 *MSC spheroids produce Col IV-positive matrices in chemically defined media*

We then asked whether the MSC spheroids cultivated in defined media contained basement membrane-type Col IV networks. Spheroids provide a physiologically relevant culture context in which 3D cell-cell interactions and biomechanical cues more closely resemble the tissue environment, in contrast to rigid 2D substrates that can bias MSCs towards fibrotic matrix production (Loomis et al., 2022; Park et al., 2023; Walker et al., 2021). Moreover, the spheroid format enables assessment of whether MSC-secreted ECM proteins are appropriately processed and assembled into organized, tissue-like basement membrane scaffolds.

302 Spheroids were decellularized using a protocol reported to preserve matrix architecture (Li et al., 2021)
303 and immunostained for fibronectin (FN) and Col IV. Multi-labelling for additional basement
304 membrane constituents was impeded by the lack of reliable commercial antibodies produced in other
305 species. Confocal imaging of the spheroids at low magnification (10X), confirmed the tissue-
306 dependent size differences documented by light microscopy (Fig. 1), but revealed complex surface
307 topology, some of which may be an artefact of deformation after mounting which implies
308 viscoelasticity (Fig. 3A). At higher magnification (40X), complementary networks of fibronectin and
309 Col IV were observed (Fig. 3B). The decellularized matrices all presented architectural basement
310 membrane features including pores, fibre alignment and rough surface topography (Fig. 3A), which
311 are more clearly depicted in digitally enlarged representative images (Fig. 3B).

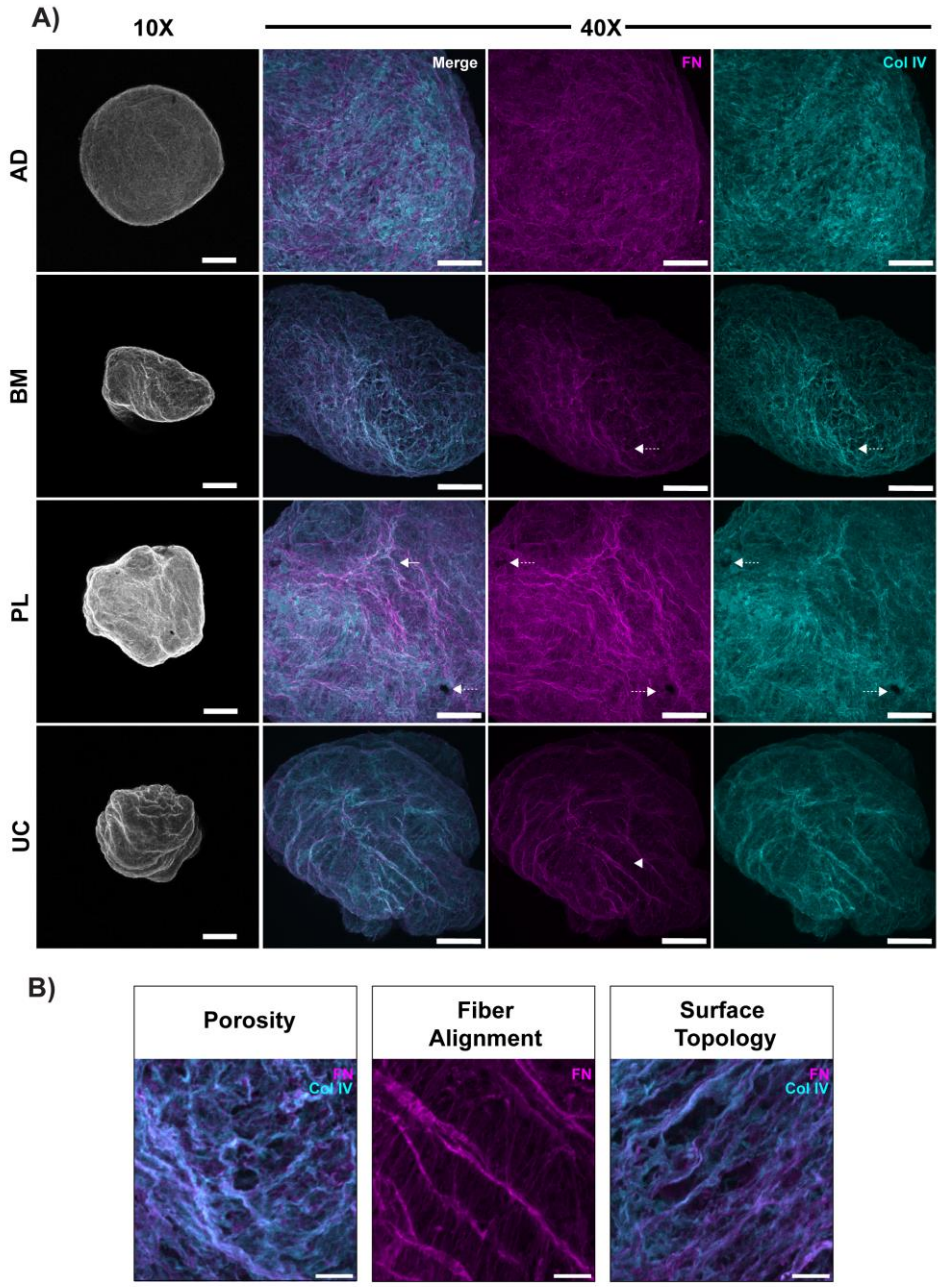

312

313 **Figure 3. MSC spheroids produce Col IV-positive matrices in chemically defined media.**

314 Whole mount confocal images of 4 day old decellularized matrices produced by spheroid cultures of
315 MSCs from adult (AD, BM) and perinatal (PL, UC) tissues. Matrices were immunostained for
316 fibronectin (FN, magenta) and Col IV (cyan). (A) Maximum intensity projection of 2μm confocal

317 images captured over a Z depth of 50μm with a 10x objective. Overlaid FN and Col IV confocal images,
318 shown in greyscale, reveal surface roughness. Some loss of circularity and folding may be due to
319 compression between the slide and the coverslip, suggesting that the scaffolds have plasticity. Scale
320 bar = 50μm. Maximum intensity projection of 0.5μm slices captured over a Z depth of 80μm with a
321 40x objective reveal complex networks of FN and Col IV. These proteins appear to be aligned in a
322 complementary fashion that moderately overlaps (white). Architectural features including pores
323 (dotted arrow), fiber directionality (arrowhead) and surface topology (arrow) are also apparent. (B)
324 Digital magnification of representative panels in (A) show enhanced architectural details including
325 defined pore structures (Porosity), alignment of fibronectin fibers across 2 planes (Fiber Alignment),
326 and rough Surface Topography featuring peaks and troughs. These topological and topographical
327 features are found in all examined spheroid-derived matrices. Representative images from 3-4 technical
328 replicates per MSC tissue source. Scale bar = 100μm.

329

330 Three-dimensional volumetric reconstruction of the confocal images revealed distinct patterns of
331 matrix organization. In the adult MSC-derived matrices, fibronectin and Col IV appeared to be
332 interwoven, while the perinatal MSC-derived matrices segregated fibronectin into apical sheets, with
333 an underlying sheet of Col IV (Fig. 4A). Regardless of their relative orientation, fibronectin and Col
334 IV rarely overlapped except at the interface between the apical and luminal matrix facets (Fig. 4B).

335

336

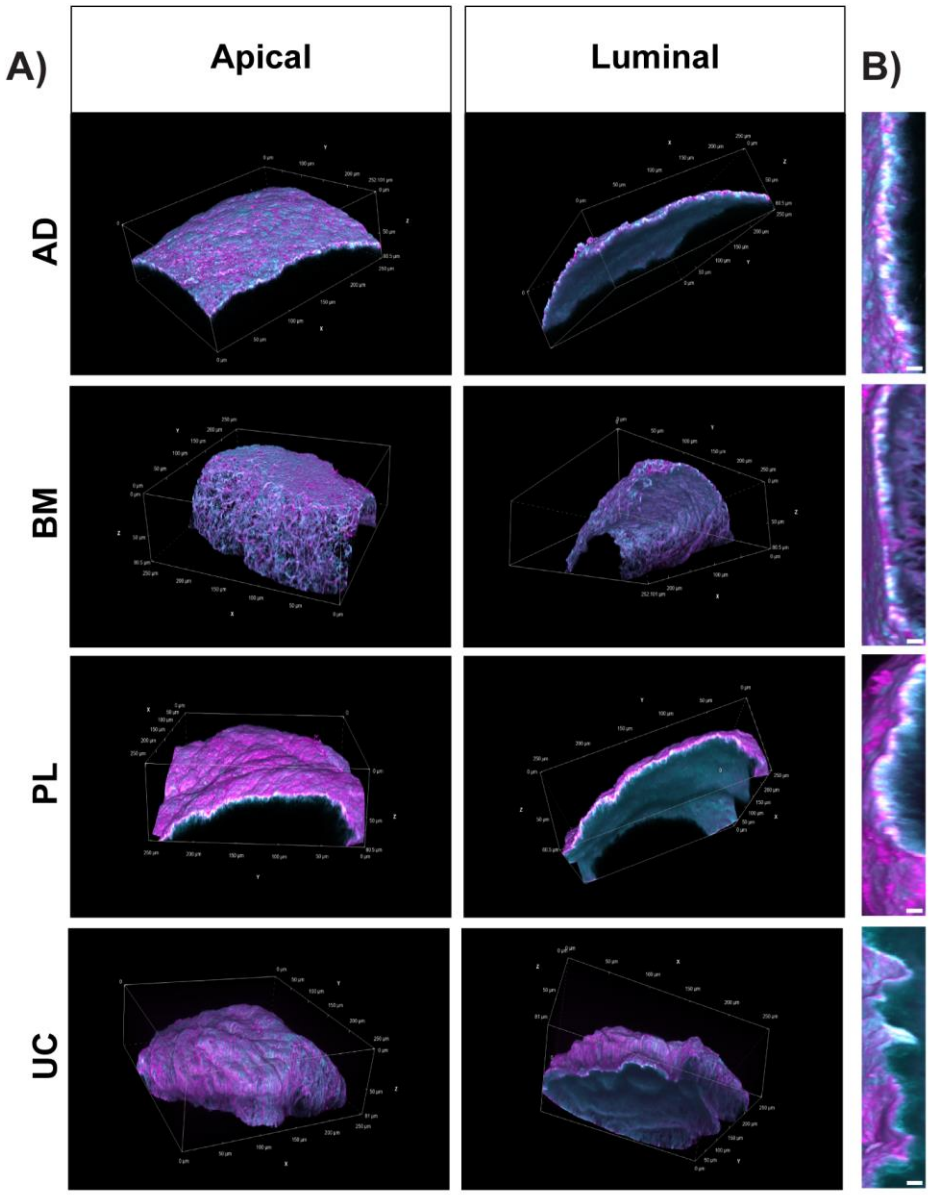

337

338 **Figure 4. Perinatal-derived MSCs produce self-assembled matrices with overlaid FN and Col IV**
339 **sheets.** Decellularized whole mount spheroid-derived matrices produced by AD, BM, PL and UC
340 MSCs were examined in volume view with alpha blending to highlight surface and compositional
341 topography. (A) Fibronectin (FN, magenta) and Col IV (cyan) appear to be interwoven in matrices
342 produced by adult MSCs (AD, BM). By contrast, the perinatal MSCs (PL, UC) establish matrices with

343 sheet-like organization, whereby FN is enriched on the apical surface, complemented by a sheet of Col
344 IV on the underlying luminal surface. (B) Cross-sections reveal a marked overlap of FN and Col IV
345 (white) at the interface of the apical and luminal sheets. Scale bar = 5μm. Representative images from
346 3-4 technical replicates per MSC source. Confocal images were captured in 0.5μm sections through a
347 Z-depth of 80μm.

348

349 3.3 *Self-assembled MSC matrices contain canonical basement membrane factors*

350 Having shown that MSC-derived matrices contain networked fibronectin and Col IV, we used western
351 blot to assess whether other basement membrane factors were also present. Decellularized spheroids
352 were solubilized, normalized to total protein, size fractionated and then immunoblotted for fibronectin,
353 laminin β/γ, Col IV, Col VIα1 and elastin (Fig. 5). Laminin β and γ chains, along with an α chain,
354 form the basic heterotrimeric structure of all laminins. They assemble with other proteins, such as Col
355 IV and nidogen, to create the complex, organized network of the basement membrane (Lennon &
356 Sherwood, 2025; Page-McCaw & Ferrell, 2025; Page-McCaw et al., 2025). Col VIα1 is a key
357 component of type VI collagen, which acts as a structural link between the basement membrane and
358 the surrounding interstitial matrix, providing mechanical support to tissues (Cescon et al., 2015;
359 Gregory et al., 2024). Elastin anchors cells to the matrix and provides mechanical support; it functions
360 in conjunction with other basement membrane components to provide elasticity, allowing tissues to
361 stretch and recoil (Krymchenko et al., 2025; Ruiz et al., 2024; Trębacz & Barzycka, 2023). The relative
362 abundance of these analytes differed in matrices produced by each MSC donor. BM MSC-derived
363 matrices were markedly enriched for fibronectin, while UC MSC-derived matrices were enriched for
364 all the basement membrane constituents compared to the other donors (Fig. 5). Col IV and elastin were

365 less abundant in the AD-derived scaffolds, while all the analytes except elastin were detected in PL-
366 derived matrices (Fig. 5).

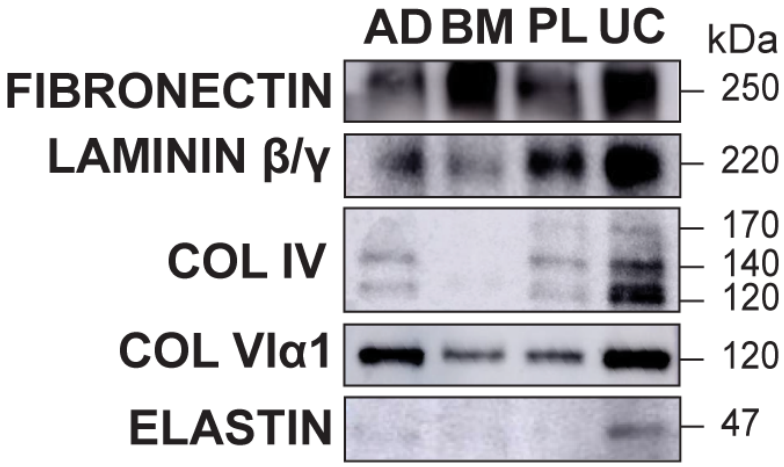

367

368 **Figure 5: MSC-derived matrices contain basement membrane-specific proteins.** Relative
369 abundance of basement membrane proteins in decellularized AD, BM, PL or UC MSC spheroids were
370 analyzed by western blot. Samples were normalized by total protein (3μg/lane). UC MSC-derived
371 matrices were enriched for the basement membrane factors Col IV, Col VIα1 and elastin. Matrix from
372 BM MSCs contained relatively more fibronectin than the other scaffolds. Representative data from
373 n=3 independent experiments.

374

375

376

377 3.4 *Multilayered UC MSCs produce-matrix-basement membrane-type sheets in defined media*

378 Having determined that the UC MSC donor produces synthesizes the most robust repertoire of
379 basement membrane proteins when cultured as spheroids (Fig. 5), we next asked whether a similar

380 basement membrane-type matrix could be generated when UC MSCs were grown as adherent cultures.
381 Compared with spheroids, multilayered cell sheets are technically simpler and may offer greater
382 reproducibility and scalability. However, adherence to rigid culture substrates imposes a stiffer
383 microenvironment and reduces 3D cell-cell interactions, conditions that are known to influence matrix
384 deposition and may preferentially promote interstitial rather than basement membrane matrix
385 production. We therefore sought to determine whether basement membrane assembly is preserved
386 under these 2D culture conditions.

387 UC MSCs were cultured in adherent multilayers followed by decellularization to assess ECM
388 biogenesis. We then analyzed the deposition of select adhesive (fibronectin, laminin β/γ) and structural
389 (Col IV, Col VIα1) basement membrane proteins over time by immunofluorescence. Fibronectin was
390 the most prevalent matrix component at Day 1 and increased in abundance and architectural complexity
391 through Day 7 (Fig. 6A, B). Col IV and Col VIα1 were barely detectable at Day 2 and continued to
392 accumulate in networked structures through Day 7 (Fig. 6A, B). At Day 7, laminin β/γ was the last
393 analyte to be detected. The matrix sheets were 8-10μm thick on Day 7, as determined using cross-
394 sections of Z-stacked images (Fig. 6C). In cellularized samples, networked fibronectin (red) is seen
395 connecting with and intercalating between MSCs (white) highly expressing the Col IV cross-linking
396 enzyme lysyl oxidase-like 2 (LOXL2; Fig. 6C, D).

397

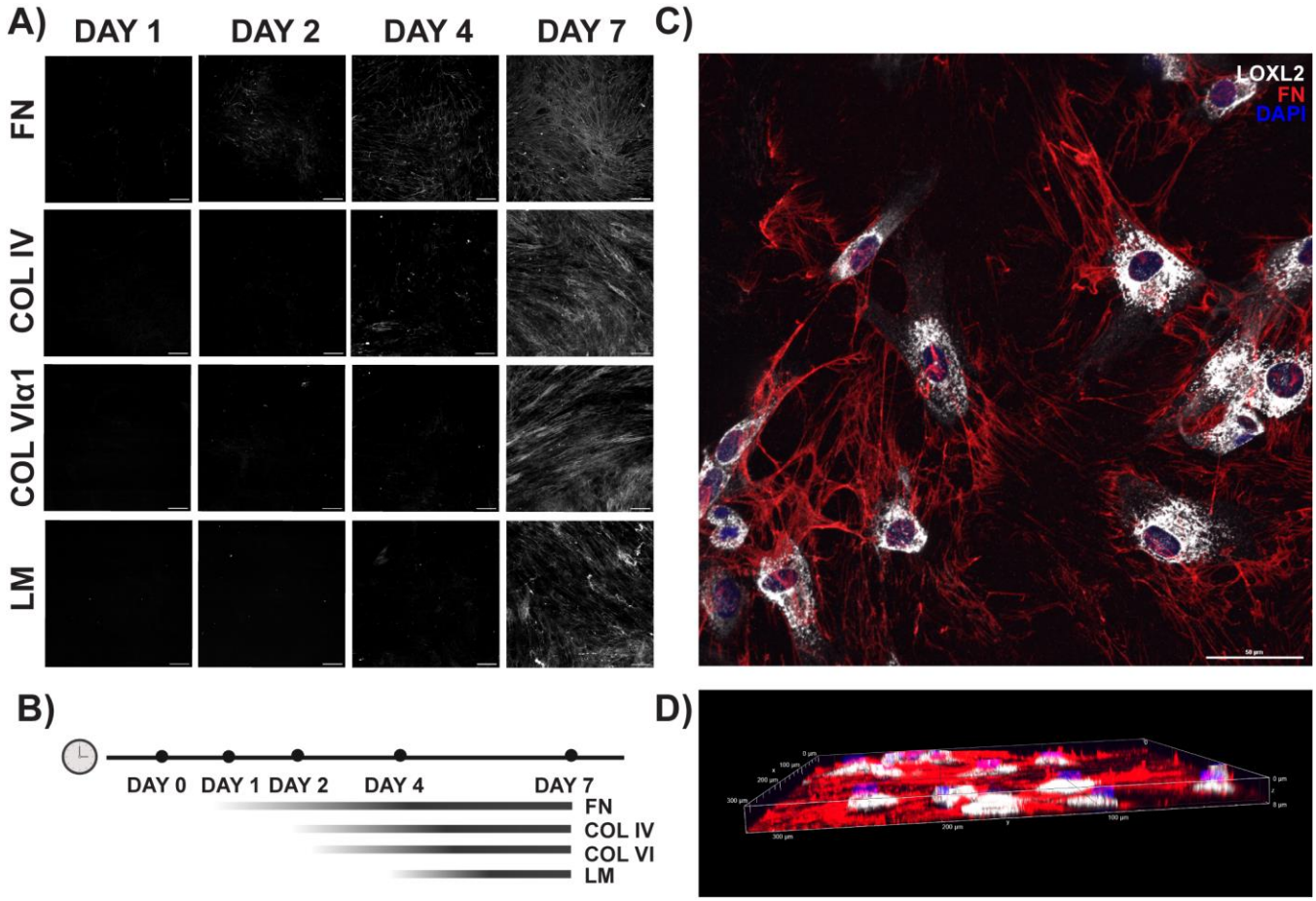

Figure 6: Multilayered UC MSCs construct sheets of scaffolded matrix.

(A) Fibronectin (FN) is first detected by immunogenic staining 2 days after seeding, followed by Col IV on Day 4. Col VIα1 and laminin (LM) are not readily detected until Day 7, when all 4 analytes are visible components of a networked matrix structure. Scale bar = 100µm (B) Schematic summarizing the temporal incorporation of ECM components depicted in (A). (C) Maximum intensity projection 4-day MSC multilayers show networks of fibronectin (FN; red) intercalating between MSCs expressing high levels of the Col IV cross-linking enzyme LOXL2 (white), in (D) a matrix 8µm thick. Data shown is representative from a dataset of n=3 independent experiments with 5-6 fields of view per experiment.

408 3.5 *UC MSCs matrix sheets are amenable to recellularization*

409 Finally, we asked whether MSC-derived matrices were amenable to recellularization and could support
410 cell-matrix interactions. Matrix sheets proved more practical and efficient than spheroids for reseeding
411 and were selected for this experiment. Fluorescent labeled UC MSCs were incubated overnight with
412 decellularized matrix sheets immunostained to visualize fibronectin. The next day, cell-matrix
413 interactions were assessed by time lapse imaging. MSCs successfully adhered to the nascent scaffolds
414 (Fig. 7). Time-lapse microscopy showed MSCs attached to the fibronectin fibers. MSCs appeared to
415 leverage this matrix interaction to migrate through focal planes of the matrix (Fig. 7A) by pulling or
416 tugging on the flexible fibronectin fibers (Fig. 7B, Movie S1). In preliminary studies, matrix produced
417 by MSC in our animal component-free workflow can support the adhesion, migration and proliferation
418 of other cell types including human neural progenitor cells, human umbilical vein endothelial cells and
419 fibroblasts (not shown). Taken together, this study establishes MSCs as a viable and ethically favorable
420 source for the generation of self-assembling matrix proteins, including basement membrane
421 components, in chemically defined conditions.

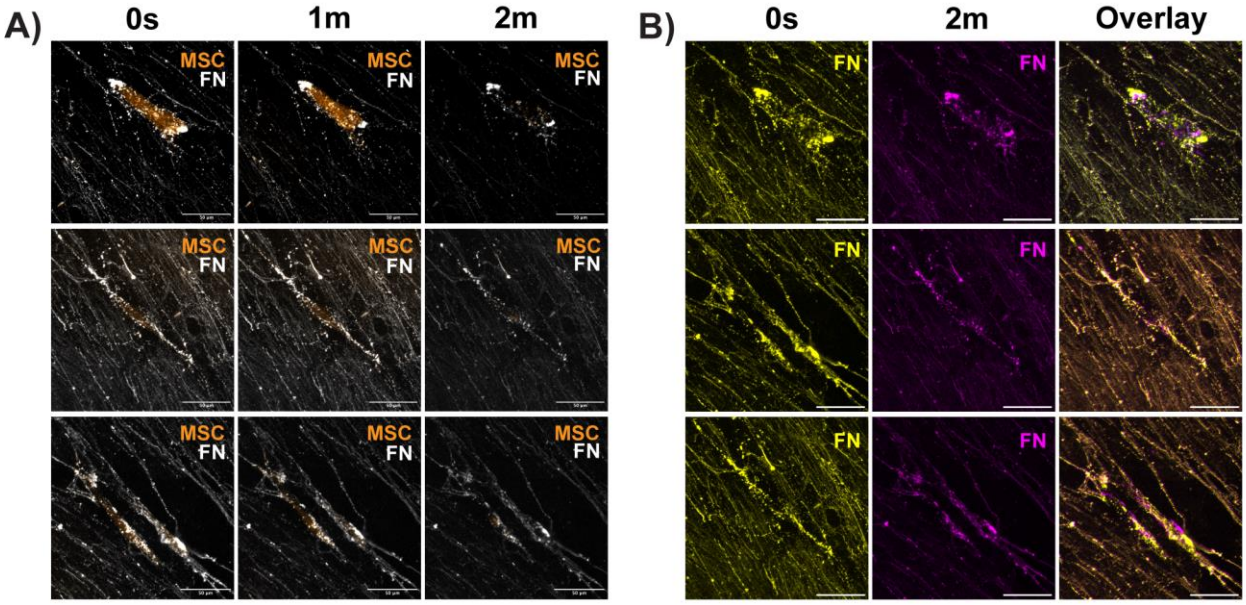

Figure 7: UC MSC derived matrix sheets can be colonized by new cells. Decellularized UC MSC sheets, produced in chemically defined media, support interactive cell migration of newly introduced UC MSCs **(Movie S1).** (A) In representative time lapse images, MSCs (orange) can be seen moving through the Z plane of scaffolded fibronectin (FN; white). FN scaffolds were false colored at 2 timepoints (0s, yellow; 2m, magenta) and overlaid to detect FN movement. The presence of unblended FN signal in cell-occupied regions shows relocation of FN, indicating dynamic cell-matrix interactions. Blended color (orange) in the unoccupied scaffold areas suggests that FN remains static in the absence of cell movement. Scale bar = 50µm.

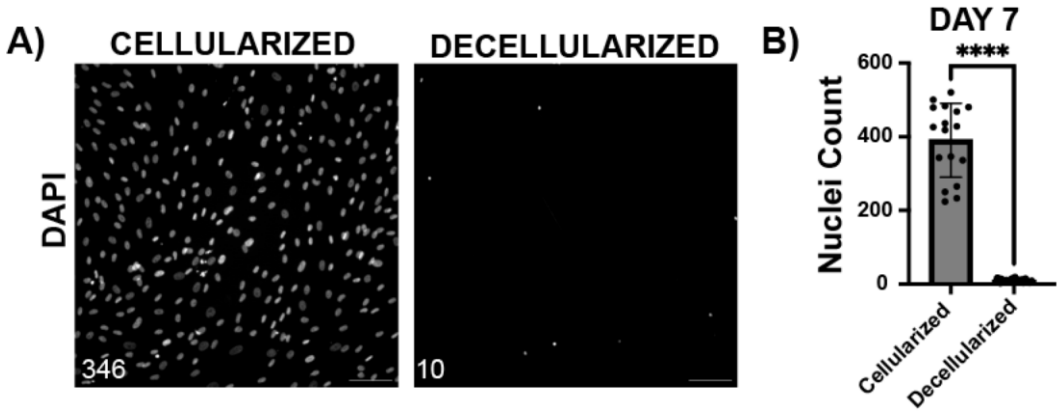

Figure S1: Ammonium hydroxide decellularization efficiently clears nuclear and cytoplasmic material.

Multilayered UC MSC sheets were decellularized on Day 4 (A) and Day 7 (C) after seeding using an ammonium hydroxide protocol. A) Adhered UC MSCs were labeled using DAPI (nucleus) and anti-CML antibody to detect carboxymethyl lysine residues in the nucleus and cytoplasm. Negligible signal was detected on either channel following ammonium hydroxide-based decellularization, indicating efficient clearance of nuclear and cytoplasmic material. (B) Nuclei were labeled using DAPI and quantified (number in the bottom left of the image). (C) The number of nuclei was significantly reduced by 95.8% after decellularization. Representative data from n=3 independent experiments. Scale bar = 100µm.

4 Discussion

448 There is a critical need for functional human matrix components to support the next generation of high-
449 fidelity tissue models for experimental use and transplant (Catarino et al., 2022; Liu et al., 2023;
450 Naderi-Meshkin et al., 2023; Schneider et al., 2023). Moreover, there is a paucity of intact and
451 functional basement membrane biomaterials to recapitulate the complexity of human tissues, and more
452 importantly, to facilitate vascularization (Chan et al., 2016; Marrella et al., 2018; Minor & Coulombe,
453 2020; Zhao et al., 2022). Here we report that human MSCs, which occupy perivascular niches *in vivo*
454 (Caplan, 2017; Corselli et al., 2013; Kang et al., 2010), can be leveraged to synthesize functional
455 basement membrane components in a defined, animal component-free bioprocess. The development
456 of an animal-component-free platform based on human MSCs offers a renewable and physiologically
457 relevant strategy for scalable ECM production, reducing reliance on ethically contentious animal-
458 derived materials, lowering the environmental burden associated with animal agriculture, and
459 minimizing the risk of xenogeneic contamination.

460 Our findings align with previous studies that demonstrate origin-specific synthesis of ECM factors by
461 MSCs, although this study is not sufficiently powered to statistically correlate MSC tissue source with
462 ECM composition. In previous transcriptome studies that span multiple MSC donors and origins, we
463 found that UC MSCs express significantly higher levels of the non-fibrillar basement membrane
464 collagens (Col IV and Col VI) than fibroblasts (Wiese & Braid, 2020) and BM MSCs (Wiese et al.,
465 2022). Similarly, Ragelle et al., 2017 found that decellularized neonatal dermal fibroblast-derived
466 matrices possessed less total collagen than AD and BM MSC-derived scaffolds. The most abundant
467 structural components in those BM MSC-derived scaffolds were Col I and Col VI, while Col II, III and
468 IV were present at lower levels (Ragelle et al., 2017). These results were consistent across all 5 donors
469 (Ragelle et al., 2017). Another group reported that decellularized BM MSC scaffolds contained Col
470 IV, while AD MSC scaffolds did not (Marinkovic et al., 2020), which contradicts our findings. Amable

471 *et al.* compared ECM components secreted by AD, BM and UC MSCs, finding that UC MSCs did not
472 produce detectable amounts of laminin, fibronectin, Col II, or IV. In their study AD MSCs were the
473 only MSC population to secrete Col IV at detectable concentrations, and they also produced more Col
474 I, II and III than BM and UC MSCs (Amable et al., 2014). It is plausible to expect that these disparate
475 outcomes are the consequence of different media formulations used in these studies, including FBS
476 supplemented, (Amable et al., 2014; Bartosh et al., 2010; Cesarz & Tamama, 2016; Chen et al., 2025;
477 Chiang et al., 2021; Fuentes et al., 2022; Lee et al., 2016; Marinkovic et al., 2020; Ragelle et al., 2017;
478 Yin et al., 2024), serum-free (Choi et al., 2021; Rakian et al., 2015), and xeno-free products (Bauman
479 et al., 2018; Parvin Nejad et al., 2023). This study aimed to test whether MSCs are capable of
480 synthesizing basement membrane–type matrices under chemically defined culture conditions that
481 exclude the rich array of growth factors, adhesion factors, and stabilizing components found in serum
482 or hPL-supplemented media (Delabie et al., 2025; Hodges & Melcher, 1976; Karnieli et al., 2017;
483 Klinker et al., 2017; Oikonomopoulos et al., 2015).

484 In mammals, Col IV is encoded by a family of six genes (*COL4A*1–6) that produce discrete Col IV α-
485 chains (α1–α6) (Page-McCaw & Ferrell, 2025; Page-McCaw et al., 2025). These α-chains can give
486 rise to three supramolecular scaffolds: Col IV$^{\alpha121}$, Col IV$^{\alpha345}$, and Col IV$^{\alpha121-\alpha556}$, which form networks
487 with different structural and biomechanical properties (Page-McCaw & Ferrell, 2025; Page-McCaw et
488 al., 2025). Expression of the *COL4A* genes differs between tissues and shifts during development,
489 resulting in the formation of functionally specialized basement membranes throughout the body (Page-
490 McCaw & Ferrell, 2025; Page-McCaw et al., 2025). The observation that MSCs from different tissues
491 produce distinct Col IV α-chains was therefore not unexpected and is consistent with published reports.
492 For example, we previously compared the transcriptome profiles of 3 donors each of UC and BM
493 MSCs and their responses to cytokine stimulation. In that study, unstimulated BM MSCs, as used here,

494 expressed very high levels of *COL4*A1 and *COL4*A2 and very low levels of *COL4*A5, and did not
495 express *COL4*A3, *COL4*A4 or *COL4*A6 (Wiese et al., 2022). UC MSCs expressed even higher levels
496 of *COL4*A1 and *COL4*A2, moderate levels of *COL4*A5 and low levels of *COL4*A3, *COL4*A4 and
497 *COL4*A6 (Wiese et al., 2022). Notably, expression of these genes did not vary significantly between
498 donor populations and were consistent with an earlier study using other UC MSC donors cultured in a
499 different media formulation (Wiese et al., 2019). These data imply that Col IV synthesized by BM
500 MSCs may only form Col IV$^{\alpha121}$ scaffolds, while UC MSCs synthesize the starting material for all 3
501 Col IV supramolecular structures and warrants further study.

502 These unique properties may contribute to the apparent differences in volumetric Col IV scaffolding,
503 where the Col IV and fibronectin networks constructed by BM MSC spheroids (Fig. 3A, second row)
504 appeared less dense than the perinatal MSC-derived matrices (Fig. 3A, bottom rows). Indeed, the
505 highly stringent glomerular basement membrane in the kidney, which filters urine to eliminate waste
506 while retaining proteins and other useful molecules contains two Col IV networks – a Col
507 IV$^{\alpha121}$ network and a Col IV$^{\alpha345}$ network (Page-McCaw et al., 2025). Our gene expression data
508 indicates that UC MSCs can synthesize both networks, as well as Col IV$^{\alpha121-\alpha556}$**,** which would yield a
509 more stringent Col IV network than the BM MSCs which can only produce a Col IV$^{\alpha121}$ network
510 (Wiese et al., 2022).

511 Compaction is a natural developmental process that indicates organotypic self-organization (Baker &
512 Chen, 2012; Domnina et al., 2020). Spontaneous compaction, as observed in this study (Fig. 1), is
513 driven by ECM structure and stiffness (Efremov et al., 2021; Jahin et al., 2023; Kosheleva et al., 2023),
514 actin contractility (Lee et al., 2019; Sart et al., 2014; Sharma et al., 2025; Tsai et al., 2015; Turlier &
515 Maître, 2015), cell-matrix adhesion (Bartosh et al., 2013; Yokomine et al., 2025) and availability of
516 matrix remodeling enzymes (van der Net et al., 2024; Yokomine et al., 2025). Here, we found that the

517 BM MSC-derived spheroids were significantly more compact than the perinatal or adipose-derived
518 MSC spheroids (Fig. 1), which could be the result of several key differences. The protein composition
519 of the BM MSC matrices varied the most from the other tissue sources (Fig. 5), and they also exhibited
520 a more open network of fibronectin and Col IV (Fig. 3A, Fig. 4A). These data suggest that the BM
521 MSC-derived matrices may have different biomechanics than the matrices derived from the AD, UC
522 and PL MSC donors, which we are currently assessing using biophysical techniques like atomic force
523 microscopy and optical tweezers.

524 The rate of cell proliferation may also differ between MSC spheroids, leading to differences in cell
525 density with consequent effects on compaction. A previous study showed that as the number of MSCs
526 per spheroid increases, the packing density decreases, resulting in tightly packed, smaller spheroids
527 and loosely packed, larger spheroids (Murphy et al., 2017). It is possible that variations in proliferation
528 rates between spheroids, and thus differences in cell number over time, correlates with their
529 compaction. In addition, analysis using spheroids derived from numerous donors of each sex would
530 help discern whether different compaction rates are the result of tissue-imprinted variables or biological
531 differences between donors irrespective of the tissue of origin.

532 We performed a temporal analysis of ECM deposition by MSCs cultured in multilayered sheets at
533 different timepoints, studies that are reportedly under-represented in the literature (Fuentes et al.,
534 2022). A previous study, using human AD MSCs cultured in DMEM/F12 plus FBS, found that matrix
535 assembly was slower in sheet cultures than in spheroids, whereby laminin and Col IV were barely
536 detectable in the ECM after 4 days although the MSCs stained brightly, suggesting that secretion of
537 these proteins was just initiating (Glazieva et al., 2023). This agrees with our data, where Col IV was
538 readily detected by ICC in matrices isolated from 4-day old spheroids (Fig. 3), when it was barely
539 discernible in matrices from 4-day old MSC multilayers (Fig. 6A, B). Despite the relative delay in

540 matrix assembly, the multilayered MSCs sheets established their ECM in a temporal sequence of
541 developmental basement membrane assembly, starting with a fibronectin network (Fig. 6A, B). This
542 foundational scaffold was then elaborated with laminin, Col IV, Col VI and additional fibronectin,
543 recapitulating the hierarchical pattern of basement membrane assembly *in vivo* (Pompili et al., 2021).
544 In-depth characterization of the MSC-derived matrices using proteomics is necessary to fully
545 appreciate and compare the complement of adhesion, structural, proteoglycan, instructive and signaling
546 components and their assembly. However, analysis of decellularized matrices is not straightforward,
547 since conventional preparation procedures can lead to artefacts in the data, while matrisome analysis
548 from cellularized samples is not sufficiently enriched to detect low abundance proteins (Byron et al.,
549 2013; Diedrich et al., 2024; Frattini et al., 2024; Monteiro-Lobato et al., 2022; Naba, 2023; Ouni et al.,
550 2020).

551 Environmental conditions like oxygen tension also influence matrix synthesis (Kumar et al., 2018; Lee
552 et al., 2016; Satyam et al., 2016). For example, a recent study showed that human articular
553 chondrocytes cultured at physiological oxygen tension (5% O_2) produced thicker matrices with
554 increased deposition of glycosaminoglycans and Col II as well as increased tensile strength (Dennis et
555 al., 2020). MSC spheroids cultured under hypoxia (2% O_2) produced more laminin, fibronectin and
556 Col I compared to spheroids cultured at ambient (~20%) O_2 (Shearier et al., 2016). Since MSCs were
557 cultivated under 5% O_2 in our study, oxygen tension may be a key differential that contributes to the
558 disparate outcomes between our data and other studies that maintain MSCs at ambient O_2 tension.

559 Decellularized matrices derived from MSC spheroids and cell-sheet cultures represent biologically
560 relevant scaffolds that preserve native extracellular matrix architecture, growth-factor–binding
561 capacity, and integrin-specific adhesion cues – features that are essential for supporting cell survival
562 and directing lineage specification in engineered tissues. Here we provide proof-of-concept that human

563 MSCs cultured in a chemically defined bioprocess can produce basement membrane components that
564 self-assemble into spheroid and sheet-type matrices. These naturally formed scaffolds can be effective
565 recellularized with other cell types, demonstrating the functional integrity of the MSC-derived matrix
566 proteins. While purified collagens, including Col I and Col IV, are known to self-assemble into
567 matrices *in vitro* (Al-Shaer & Forde, 2025; Kotch & Raines, 2006; Yu et al., 2024), it remains unclear
568 whether more complex matrices comprising multiple basement membrane proteins can similarly self-
569 assemble outside the cellular context. Collectively, these findings advance the development of high
570 fidelity, human-derived tissue models for disease modeling, drug discovery and regenerative medicine,
571 while supporting sustainable and ethically responsible biomedical research.

572 Conflict of Interest

573 LRB is founder and CSO of Aurora BioSolutions Inc. SNS has no conflicts to declare. The authors
574 declare that the research was conducted in the absence of any commercial or financial relationships
575 that could be construed as a potential conflict of interest.

576 **4 Author Contributions**

577 SNS: Collection and/or assembly of data, data analysis and interpretation, manuscript writing, critical
578 review of the manuscript and final approval of manuscript. LRB: Conception/design, assembly of data,
579 data analysis and interpretation, manuscript writing, critical review of the manuscript and final
580 approval of manuscript.

581

582 **5 Funding**

583 This project was funded by an NSERC Discovery Grant to LRB. Additional operating funds were
584 provided by a Canada Research Chair (Tier 2) in MSC Biology awarded to LRB.

585

586 **6 Acknowledgements**

587 The authors would like to acknowledge Tissue Regeneration Therapeutics Inc. (TRT), Toronto,
588 Canada, for provision of human umbilical cord perivascular cells. The authors would also like to thank
589 Braid lab members Dr. Simon Wang for his technical assistance with confocal imaging, Dr. Alaa Al-
590 Shaer for editing the final version of the manuscript, Daniel Sloseris for characterizing decellularization
591 efficiency and Ana Gibbert for her early optimization of the MSC spheroid cultures.

592

593

594

595

596

7 References

Aisenbrey, E. A., & Murphy, W. L. (2020). Synthetic alternatives to Matrigel. *Nature Reviews. Materials*, *5*(7), 539–551. https://doi.org/10.1038/s41578-020-0199-8

Al-Shaer, A., & Forde, N. R. (2025). Decoding collagen's thermally induced unfolding and refolding pathways. *Proceedings of the National Academy of Sciences*, *122*(20), e2420308122. https://doi.org/10.1073/pnas.2420308122

Amable, P. R., Teixeira, M. V. T., Carias, R. B. V., Granjeiro, J. M., & Borojevic, R. (2014). Protein synthesis and secretion in human mesenchymal cells derived from bone marrow, adipose tissue and Wharton's jelly. *Stem Cell Research & Therapy*, *5*(2), 53. https://doi.org/10.1186/scrt442

Baker, B. M., & Chen, C. S. (2012). Deconstructing the third dimension – how 3D culture microenvironments alter cellular cues. *Journal of Cell Science*, *125*(13), 3015–3024. https://doi.org/10.1242/jcs.079509

Baker, M. (2016a). 1,500 scientists lift the lid on reproducibility. *Nature*, *533*(7604), 452–454. https://doi.org/10.1038/533452a

Baker, M. (2016b). Reproducibility: Respect your cells! *Nature*, *537*(7620), 433–435. https://doi.org/10.1038/537433a

Bartosh, T. J., Ylöstalo, J. H., Bazhanov, N., Kuhlman, J., & Prockop, D. J. (2013). Dynamic compaction of human mesenchymal stem/precursor cells (MSC) into spheres self-activates caspase-dependent IL1 signaling to enhance secretion of modulators of inflammation and immunity (PGE2, TSG6 and STC1). *Stem Cells (Dayton, Ohio)*, *31*(11), 10.1002/stem.1499. https://doi.org/10.1002/stem.1499

619 Bartosh, T. J., Ylöstalo, J. H., Mohammadipoor, A., Bazhanov, N., Coble, K., Claypool, K., Lee, R.
620 H., Choi, H., & Prockop, D. J. (2010). Aggregation of human mesenchymal stromal cells
621 (MSCs) into 3D spheroids enhances their antiinflammatory properties. *Proceedings of the*
622 *National Academy of Sciences*, *107*(31), 13724–13729.
623 https://doi.org/10.1073/pnas.1008117107

624 Bauman, E., Feijão, T., Carvalho, D. T. O., Granja, P. L., & Barrias, C. C. (2018). Xeno-free pre-
625 vascularized spheroids for therapeutic applications. *Scientific Reports*, *8*(1), 230.
626 https://doi.org/10.1038/s41598-017-18431-6

627 Byron, A., Humphries, J. D., & Humphries, M. J. (2013). Defining the extracellular matrix using
628 proteomics. *International Journal of Experimental Pathology*, *94*(2), 75–92.
629 https://doi.org/10.1111/iep.12011

630 Caplan, A. I. (2017). New MSC: MSCs as pericytes are Sentinels and gatekeepers. *Journal of*
631 *Orthopaedic Research: Official Publication of the Orthopaedic Research Society*, *35*(6),
632 1151–1159. https://doi.org/10.1002/jor.23560

633 Catarino, C. M., Kaiser, K., Baltazar, T., Catarino, L. M., Brewer, J. R., & Karande, P. (2022).
634 Evaluation of native and non-native biomaterials for engineering human skin tissue.
635 *Bioengineering & Translational Medicine*, *7*(3), e10297. https://doi.org/10.1002/btm2.10297

636 Cesarz, Z., & Tamama, K. (2016). Spheroid Culture of Mesenchymal Stem Cells. *Stem Cells*
637 *International*, *2016*, 9176357. https://doi.org/10.1155/2016/9176357

638 Cescon, M., Gattazzo, F., Chen, P., & Bonaldo, P. (2015). Collagen VI at a glance. *Journal of Cell*
639 *Science*, *128*(19), 3525–3531. https://doi.org/10.1242/jcs.169748

640 Chan, E. C., Kuo, S.-M., Kong, A. M., Morrison, W. A., Dusting, G. J., Mitchell, G. M., Lim, S. Y.,
641 & Liu, G.-S. (2016). Three Dimensional Collagen Scaffold Promotes Intrinsic Vascularisation
642 for Tissue Engineering Applications. *PLOS ONE*, *11*(2), e0149799.
643 https://doi.org/10.1371/journal.pone.0149799

644 Chen, G. H., Sia, K.-C., Liu, S.-W., Kao, Y.-C., Yang, P.-C., Ho, C.-H., Huang, S.-C., Lee, P.-Y.,
645 Liang, M.-Z., Chen, L., & Huang, C.-C. (2025). Implantation of MSC spheroid-derived 3D
646 decellularized ECM enriched with the MSC secretome ameliorates traumatic brain injury and
647 promotes brain repair. *Biomaterials*, *315*, 122941.
648 https://doi.org/10.1016/j.biomaterials.2024.122941

649 Chiang, C.-E., Fang, Y.-Q., Ho, C.-T., Assunção, M., Lin, S.-J., Wang, Y.-C., Blocki, A., & Huang,
650 C.-C. (2021). Bioactive Decellularized Extracellular Matrix Derived from 3D Stem Cell
651 Spheroids under Macromolecular Crowding Serves as a Scaffold for Tissue Engineering.
652 *Advanced Healthcare Materials*, *10*(11), e2100024. https://doi.org/10.1002/adhm.202100024

653 Choi, J., Choi, W., Joo, Y., Chung, H., Kim, D., Oh, S. J., & Kim, S.-H. (2021). FGF2-primed 3D
654 spheroids producing IL-8 promote therapeutic angiogenesis in murine hindlimb ischemia.
655 *NPJ Regenerative Medicine*, *6*, 48. https://doi.org/10.1038/s41536-021-00159-7

656 Corselli, M., Crisan, M., Murray, I. R., West, C. C., Scholes, J., Codrea, F., Khan, N., & Péault, B.
657 (2013). Identification of perivascular mesenchymal stromal/stem cells by flow cytometry.
658 *Cytometry. Part A: The Journal of the International Society for Analytical Cytology*, *83*(8),
659 714–720. https://doi.org/10.1002/cyto.a.22313

660 Delabie, W., Vandewalle, V., Seghers, S., De Bleser, D., Vandekerckhove, P., & Feys, H. B. (2025).
661 Comparison of culture media supplements identifies serum components in self-reported

662 serum-free preparations. *Stem Cell Research & Therapy*, *16*, 454.
663 https://doi.org/10.1186/s13287-025-04561-6

664 Dennis, J. E., Whitney, G. A., Rai, J., Fernandes, R. J., & Kean, T. J. (2020). Physioxia Stimulates
665 Extracellular Matrix Deposition and Increases Mechanical Properties of Human Chondrocyte-
666 Derived Tissue-Engineered Cartilage. *Frontiers in Bioengineering and Biotechnology*, *8*.
667 https://doi.org/10.3389/fbioe.2020.590743

668 Diedrich, A.-M., Daneshgar, A., Tang, P., Klein, O., Mohr, A., Onwuegbuchulam, O. A., von
669 Rueden, S., Menck, K., Bleckmann, A., Juratli, M. A., Becker, F., Sauer, I. M., Hillebrandt,
670 K. H., Pascher, A., & Struecker, B. (2024). Proteomic analysis of decellularized mice liver
671 and kidney extracellular matrices. *Journal of Biological Engineering*, *18*(1), 17.
672 https://doi.org/10.1186/s13036-024-00413-8

673 Domnina, A., Ivanova, J., Alekseenko, L., Kozhukharova, I., Borodkina, A., Pugovkina, N.,
674 Smirnova, I., Lyublinskaya, O., Fridlyanskaya, I., & Nikolsky, N. (2020). Three-Dimensional
675 Compaction Switches Stress Response Programs and Enhances Therapeutic Efficacy of
676 Endometrial Mesenchymal Stem/Stromal Cells. *Frontiers in Cell and Developmental*
677 *Biology*, *8*, 473. https://doi.org/10.3389/fcell.2020.00473

678 Duisit, J., Amiel, H., Wüthrich, T., Taddeo, A., Dedriche, A., Destoop, V., Pardoen, T., Bouzin, C.,
679 Joris, V., Magee, D., Vögelin, E., Harriman, D., Dessy, C., Orlando, G., Behets, C., Rieben,
680 R., Gianello, P., & Lengelé, B. (2018). Perfusion-decellularization of human ear grafts
681 enables ECM-based scaffolds for auricular vascularized composite tissue engineering. *Acta*
682 *Biomaterialia*, *73*, 339–354. https://doi.org/10.1016/j.actbio.2018.04.009

683 Efremov, Y. M., Zurina, I. M., Presniakova, V. S., Kosheleva, N. V., Butnaru, D. V., Svistunov, A.
684 A., Rochev, Y. A., & Timashev, P. S. (2021). Mechanical properties of cell sheets and

685 spheroids: The link between single cells and complex tissues. *Biophysical Reviews*, *13*(4),
686 541–561. https://doi.org/10.1007/s12551-021-00821-w

687 Fonseca, V. C., Van, V., & Ip, B. C. (2023). *Primary Human Cell-Derived Extracellular Matrix from*
688 *Decellularized Fibroblast Microtissues with Tissue-Dependent Composition and*
689 *Microstructure* (p. 2023.08.15.553420). bioRxiv. https://doi.org/10.1101/2023.08.15.553420

690 Franco-Barraza, J., Beacham, D. A., Amatangelo, M. D., & Cukierman, E. (2016). Preparation of
691 Extracellular Matrices Produced by Cultured and Primary Fibroblasts. *Current Protocols in*
692 *Cell Biology*, *71*, 10.9.1-10.9.34. https://doi.org/10.1002/cpcb.2

693 Frattini, T., Devos, H., Makridakis, M., Roubelakis, M. G., Latosinska, A., Mischak, H., Schanstra, J.
694 P., Vlahou, A., & Saulnier-Blache, J.-S. (2024). Benefits and limits of decellularization on
695 mass-spectrometry-based extracellular matrix proteome analysis of mouse kidney.
696 *PROTEOMICS*, *24*(17), 2400052. https://doi.org/10.1002/pmic.202400052

697 Fuentes, P., Torres, M. J., Arancibia, R., Aulestia, F., Vergara, M., Carrión, F., Osses, N., &
698 Altamirano, C. (2022). Dynamic Culture of Mesenchymal Stromal/Stem Cell Spheroids and
699 Secretion of Paracrine Factors. *Frontiers in Bioengineering and Biotechnology*, *10*, 916229.
700 https://doi.org/10.3389/fbioe.2022.916229

701 Glazieva, V. S., Alexandrushkina, N. A., Nimiritsky, P. P., Kulebyakina, M. A., Eremichev, R. Y., &
702 Makarevich, P. I. (2023). Extracellular Matrix Deposition Defines the Duration of Cell Sheet
703 Assembly from Human Adipose-Derived MSC. *International Journal of Molecular Sciences*,
704 *24*(23), 17050. https://doi.org/10.3390/ijms242317050

705 Gonzalez-Fernandez, T., Tenorio, A. J., Saiz, A. M., & Leach, J. K. (2022). Engineered Cell-Secreted
706 Extracellular Matrix Modulates Cell Spheroid Mechanosensing and Amplifies Their

Response to Inductive Cues for the Formation of Mineralized Tissues. *Advanced Healthcare Materials*, *11*(10), e2102337. https://doi.org/10.1002/adhm.202102337

Gregory, C. A., Ma, J., & Lomeli, S. (2024). The coordinated activities of collagen VI and XII in maintenance of tissue structure, function and repair: Evidence for a physical interaction. *Frontiers in Molecular Biosciences*, *11*. https://doi.org/10.3389/fmolb.2024.1376091

Hemeda, H., Giebel, B., & Wagner, W. (2014). Evaluation of human platelet lysate versus fetal bovine serum for culture of mesenchymal stromal cells. *Cytotherapy*, *16*(2), 170–180. https://doi.org/10.1016/j.jcyt.2013.11.004

Hodges, G. M., & Melcher, A. H. (1976). Chemically-defined medium for growth and differentiation of mixed epithelial and connective tissues in organ culture. *In Vitro*, *12*(6), 450–459. https://doi.org/10.1007/BF02806025

Huang, J., Zhang, L., Wan, D., Zhou, L., Zheng, S., Lin, S., & Qiao, Y. (2021). Extracellular matrix and its therapeutic potential for cancer treatment. *Signal Transduction and Targeted Therapy*, *6*, 153. https://doi.org/10.1038/s41392-021-00544-0

Hughes, C. S., Postovit, L. M., & Lajoie, G. A. (2010). Matrigel: A complex protein mixture required for optimal growth of cell culture. *Proteomics*, *10*(9), 1886–1890. https://doi.org/10.1002/pmic.200900758

Im, G.-B., Kim, S.-W., & Bhang, S. H. (2021). Fortifying the angiogenic efficacy of adipose derived stem cell spheroids using spheroid compaction. *Journal of Industrial and Engineering Chemistry*, *93*, 228–236. https://doi.org/10.1016/j.jiec.2020.09.027

Jahin, I., Phillips, T., Marcotti, S., Gorey, M.-A., Cox, S., & Parsons, M. (2023). Extracellular matrix stiffness activates mechanosensitive signals but limits breast cancer cell spheroid proliferation

and invasion. *Frontiers in Cell and Developmental Biology*, *11*. https://doi.org/10.3389/fcell.2023.1292775

Jain, P., Rauer, S. B., Möller, M., & Singh, S. (2022). Mimicking the Natural Basement Membrane for Advanced Tissue Engineering. *Biomacromolecules*, *23*(8), 3081–3103. https://doi.org/10.1021/acs.biomac.2c00402

Jayadev, R., & Sherwood, D. R. (2017). Basement membranes. *Current Biology*, *27*(6), R207–R211. https://doi.org/10.1016/j.cub.2017.02.006

Jin, Y., Kim, H., Min, S., Choi, Y. S., Seo, S. J., Jeong, E., Kim, S. K., Lee, H.-A., Jo, S.-H., Park, J.-H., Park, B.-W., Sim, W.-S., Kim, J.-J., Ban, K., Kim, Y.-G., Park, H.-J., & Cho, S.-W. (2022). Three-dimensional heart extracellular matrix enhances chemically induced direct cardiac reprogramming. *Science Advances*, *8*(50), eabn5768. https://doi.org/10.1126/sciadv.abn5768

Johnson, T. D., Hill, R. C., Dzieciatkowska, M., Nigam, V., Behfar, A., Christman, K. L., & Hansen, K. C. (2016). Quantification of Decellularized Human Myocardial Matrix: A Comparison of Six Patients. *Proteomics. Clinical Applications*, *10*(1), 75–83. https://doi.org/10.1002/prca.201500048

Jung, S., Sen, A., Rosenberg, L., & Behie, L. A. (2010). Identification of growth and attachment factors for the serum-free isolation and expansion of human mesenchymal stromal cells. *Cytotherapy*, *12*(5), 637–657. https://doi.org/10.3109/14653249.2010.495113

Kane, K. I. W., Lucumi Moreno, E., Lehr, C. M., Hachi, S., Dannert, R., Sanctuary, R., Wagner, C., Fleming, R. M. T., & Baller, J. (2018). Determination of the rheological properties of

750 Matrigel for optimum seeding conditions in microfluidic cell cultures. *AIP Advances*, *8*(12),
751 125332. https://doi.org/10.1063/1.5067382

752 Kang, S.-G., Shinojima, N., Hossain, A., Gumin, J., Yong, R. L., Colman, H., Marini, F., Andreeff,
753 M., & Lang, F. F. (2010). Isolation and Perivascular Localization of Mesenchymal Stem Cells
754 From Mouse Brain. *Neurosurgery*, *67*(3), 711–720.
755 https://doi.org/10.1227/01.NEU.0000377859.06219.78

756 Karnieli, O., Friedner, O. M., Allickson, J. G., Zhang, N., Jung, S., Fiorentini, D., Abraham, E.,
757 Eaker, S. S., Yong, tan K., Chan, A., Griffiths, S., Wehn, A. K., Oh, S., & Karnieli, O.
758 (2017). A consensus introduction to serum replacements and serum-free media for cellular
759 therapies. *Cytotherapy*, *19*(2), 155–169. https://doi.org/10.1016/j.jcyt.2016.11.011

760 Keppie, S. J., Mansfield, J. C., Tang, X., Philp, C. J., Graham, H. K., Önnerfjord, P., Wall, A.,
761 McLean, C., Winlove, C. P., Sherratt, M. J., Pavlovskaya, G. E., & Vincent, T. L. (2021).
762 Matrix-Bound Growth Factors are Released upon Cartilage Compression by an Aggrecan-
763 Dependent Sodium Flux that is Lost in Osteoarthritis. *Function*, *2*(5), zqab037.
764 https://doi.org/10.1093/function/zqab037

765 Khalilgharibi, N., & Mao, Y. (2021). To form and function: On the role of basement membrane
766 mechanics in tissue development, homeostasis and disease. *Open Biology*, *11*(2), 200360.
767 https://doi.org/10.1098/rsob.200360

768 Kleinman, H. K., & Martin, G. R. (2005). Matrigel: Basement membrane matrix with biological
769 activity. *Seminars in Cancer Biology*, *15*(5), 378–386.
770 https://doi.org/10.1016/j.semcancer.2005.05.004

771 Klinker, M. W., Marklein, R. A., Lo Surdo, J. L., Wei, C.-H., & Bauer, S. R. (2017). Morphological
772 features of IFN-γ-stimulated mesenchymal stromal cells predict overall immunosuppressive
773 capacity. *Proceedings of the National Academy of Sciences of the United States of America*,
774 *114*(13), E2598–E2607. https://doi.org/10.1073/pnas.1617933114

775 Kosheleva, N. V., Efremov, Y. M., Koteneva, P. I., Ilina, I. V., Zurina, I. M., Bikmulina, P. Y.,
776 Shpichka, A. I., & Timashev, P. S. (2023). Building a tissue: Mesenchymal and epithelial cell
777 spheroids mechanical properties at micro- and nanoscale. *Acta Biomaterialia, Biofabrication*
778 *with Spheroid and Organoid Materials*, *165*, 140–152.
779 https://doi.org/10.1016/j.actbio.2022.09.051

780 Kotch, F. W., & Raines, R. T. (2006). Self-assembly of synthetic collagen triple helices. *Proceedings*
781 *of the National Academy of Sciences*, *103*(9), 3028–3033.
782 https://doi.org/10.1073/pnas.0508783103

783 Kozlowski, M. T., Crook, C. J., & Ku, H. T. (2021). Towards organoid culture without Matrigel.
784 *Communications Biology*, *4*(1), 1387. https://doi.org/10.1038/s42003-021-02910-8

785 Krymchenko, R., Avila-Martinez, N., Gansevoort, M., Bakker, G.-J., Gomes, M. L. N. P., Vlig, M.,
786 Versteeg, E. M. M., Boekema, B. K. H. L., van Kuppevelt, T. H., & Daamen, W. F. (2025).
787 Collagen-elastin dermal scaffolds enhance tissue regeneration and reduce scarring in
788 preclinical models. *Materials Today Bio*, *34*, 102239.
789 https://doi.org/10.1016/j.mtbio.2025.102239

790 Kumar, P., Satyam, A., Cigognini, D., Pandit, A., & Zeugolis, D. I. (2018). Low oxygen tension and
791 macromolecular crowding accelerate extracellular matrix deposition in human corneal

792 fibroblast culture. *Journal of Tissue Engineering and Regenerative Medicine*, *12*(1), 6–18.
793 https://doi.org/10.1002/term.2283

794 Lee, J. H., Han, Y.-S., & Lee, S. H. (2016). Long-Duration Three-Dimensional Spheroid Culture
795 Promotes Angiogenic Activities of Adipose-Derived Mesenchymal Stem Cells. *Biomolecules*
796 *& Therapeutics*, *24*(3), 260. https://doi.org/10.4062/biomolther.2015.146

797 Lee, W., Kalashnikov, N., Mok, S., Halaoui, R., Kuzmin, E., Putnam, A. J., Takayama, S., Park, M.,
798 McCaffrey, L., Zhao, R., Leask, R. L., & Moraes, C. (2019). Dispersible hydrogel force
799 sensors reveal patterns of solid mechanical stress in multicellular spheroid cultures. *Nature*
800 *Communications*, *10*(1), 144. https://doi.org/10.1038/s41467-018-07967-4

801 Lennon, R., & Sherwood, D. R. (2025). Basement membranes at a glance. *Journal of Cell Science*,
802 *138*(17), jcs263947. https://doi.org/10.1242/jcs.263947

803 Li, M., Fu, T., Yang, S., Pan, L., Tang, J., Chen, M., Liang, P., Gao, Z., & Guo, L. (2021). Agarose-
804 based spheroid culture enhanced stemness and promoted odontogenic differentiation potential
805 of human dental follicle cells in vitro. *In Vitro Cellular & Developmental Biology. Animal*,
806 *57*(6), 620–630. https://doi.org/10.1007/s11626-021-00591-5

807 Liu, S., Yang, W., Li, Y., & Sun, C. (2023). Fetal bovine serum, an important factor affecting the
808 reproducibility of cell experiments. *Scientific Reports*, *13*, 1942.
809 https://doi.org/10.1038/s41598-023-29060-7

810 Loomis, T., Hu, L.-Y., Wohlgemuth, R. P., Chellakudam, R. R., Muralidharan, P. D., & Smith, L. R.
811 (2022). Matrix stiffness and architecture drive fibro-adipogenic progenitors' activation into
812 myofibroblasts. *Scientific Reports*, *12*(1), 13582. https://doi.org/10.1038/s41598-022-17852-2

813 Maia, F. R., Fonseca, K. B., Rodrigues, G., Granja, P. L., & Barrias, C. C. (2014). Matrix-driven
814 formation of mesenchymal stem cell–extracellular matrix microtissues on soft alginate
815 hydrogels. *Acta Biomaterialia*, *10*(7), 3197–3208.
816 https://doi.org/10.1016/j.actbio.2014.02.049

817 Malakpour-Permlid, A., Buzzi, I., Hegardt, C., Johansson, F., & Oredsson, S. (2021). Identification
818 of extracellular matrix proteins secreted by human dermal fibroblasts cultured in 3D
819 electrospun scaffolds. *Scientific Reports*, *11*(1), 6655. https://doi.org/10.1038/s41598-021-
820 85742-0

821 Malakpour-Permlid, A., Rodriguez, M. M., Zór, K., Boisen, A., & Oredsson, S. (2025). Advancing
822 humanized 3D tumor modeling using an open access xeno-free medium. *Frontiers in*
823 *Toxicology*, *7*. https://doi.org/10.3389/ftox.2025.1529360

824 Marinkovic, M., Tran, O. N., Block, T. J., Rakian, R., Gonzalez, A. O., Dean, D. D., Yeh, C.-K., &
825 Chen, X.-D. (2020). Native extracellular matrix, synthesized ex vivo by bone marrow or
826 adipose stromal cells, faithfully directs mesenchymal stem cell differentiation. *Matrix Biology*
827 *Plus*, *8*, 100044. https://doi.org/10.1016/j.mbplus.2020.100044

828 Marrella, A., Lee, T. Y., Lee, D. H., Karuthedom, S., Syla, D., Chawla, A., Khademhosseini, A., &
829 Jang, H. L. (2018). Engineering vascularized and innervated bone biomaterials for improved
830 skeletal tissue regeneration. *Materials Today*, *21*(4), 362–376.
831 https://doi.org/10.1016/j.mattod.2017.10.005

832 Minor, A. J., & Coulombe, K. L. K. (2020). Engineering a collagen matrix for cell-instructive
833 regenerative angiogenesis. *Journal of Biomedical Materials Research Part B: Applied*
834 *Biomaterials*, *108*(6), 2407–2416. https://doi.org/10.1002/jbm.b.34573

835 Monteiro-Lobato, G. M., Russo, P. S. T., Winck, F. V., & Catalani, L. H. (2022). Proteomic Analysis
836 of Decellularized Extracellular Matrix: Achieving a Competent Biomaterial for Osteogenesis.
837 *BioMed Research International*, *2022*, 6884370. https://doi.org/10.1155/2022/6884370

838 Motta, L. C. B., Pereira, V. M., Pinto, P. A. F., Mançanares, C. A. F., Pieri, N. C. G., de Olveira, V.
839 C., Fantinato-Neto, P., & Ambrósio, C. E. (2023). 3D culture of mesenchymal stem cells
840 from the yolk sac to generate intestinal organoid. *Theriogenology*, *209*.
841 https://doi.org/10.1016/j.theriogenology.2023.06.003

842 Muiznieks, L. D., & Keeley, F. W. (2013). Molecular assembly and mechanical properties of the
843 extracellular matrix: A fibrous protein perspective. *Biochimica et Biophysica Acta (BBA) -*
844 *Molecular Basis of Disease, Fibrosis: Translation of Basic Research to Human Disease*,
845 *1832*(7), 866–875. https://doi.org/10.1016/j.bbadis.2012.11.022

846 Murphy, K. C., Hung, B. P., Browne-Bourne, S., Zhou, D., Yeung, J., Genetos, D. C., & Leach, J. K.
847 (2017). Measurement of oxygen tension within mesenchymal stem cell spheroids. *Journal of*
848 *The Royal Society Interface*, *14*(127), 20160851. https://doi.org/10.1098/rsif.2016.0851

849 Naba, A. (2023). Ten Years of Extracellular Matrix Proteomics: Accomplishments, Challenges, and
850 Future Perspectives. *Molecular & Cellular Proteomics: MCP*, *22*(4), 100528.
851 https://doi.org/10.1016/j.mcpro.2023.100528

852 Naderi-Meshkin, H., Cornelius, V. A., Eleftheriadou, M., Potel, K. N., Setyaningsih, W. A. W., &
853 Margariti, A. (2023). Vascular organoids: Unveiling advantages, applications, challenges, and
854 disease modelling strategies. *Stem Cell Research & Therapy*, *14*(1), 292.
855 https://doi.org/10.1186/s13287-023-03521-2

856 Novoseletskaya, E., Grigorieva, O., Nimiritsky, P., Basalova, N., Eremichev, R., Milovskaya, I.,
857 Kulebyakin, K., Kulebyakina, M., Rodionov, S., Omelyanenko, N., & Efimenko, A. (2020).
858 Mesenchymal Stromal Cell-Produced Components of Extracellular Matrix Potentiate
859 Multipotent Stem Cell Response to Differentiation Stimuli. *Frontiers in Cell and*
860 *Developmental Biology*, *8*, 555378. https://doi.org/10.3389/fcell.2020.555378

861 Oikonomopoulos, A., van Deen, W. K., Manansala, A.-R., Lacey, P. N., Tomakili, T. A., Ziman, A.,
862 & Hommes, D. W. (2015). Optimization of human mesenchymal stem cell manufacturing:
863 The effects of animal/xeno-free media. *Scientific Reports*, *5*(1), 16570.
864 https://doi.org/10.1038/srep16570

865 Olesen, K., Rodin, S., Mak, W. C., Felldin, U., Österholm, C., Tilevik, A., & Grinnemo, K.-H.
866 (2021). Spatiotemporal Extracellular Matrix Modeling for in Situ Cell Niche Studies. *Stem*
867 *Cells*, *39*(12), 1751–1765. https://doi.org/10.1002/stem.3448

868 Oredsson, S., Malakpour-Permlid, A., Zhu, J., & Weber, T. (2025). Protocol for the use of Oredsson
869 universal replacement medium for cell banking and routine culturing of monolayer and
870 suspension cultures. *STAR Protocols*, *6*(2), 103781.
871 https://doi.org/10.1016/j.xpro.2025.103781

872 Ouni, E., Ruys, S. P. dit, Dolmans, M.-M., Herinckx, G., Vertommen, D., & Amorim, C. A. (2020).
873 Divide-and-Conquer Matrisome Protein (DC-MaP) Strategy: An MS-Friendly Approach to
874 Proteomic Matrisome Characterization. *International Journal of Molecular Sciences*, *21*(23),
875 9141. https://doi.org/10.3390/ijms21239141

876 Page-McCaw, A., & Ferrell, N. (2025). Basement membrane structure and function: Relating biology
877 to mechanics. *Matrix Biology*, *141*, 16–31. https://doi.org/10.1016/j.matbio.2025.08.004

878 Page-McCaw, P. S., Pokidysheva, E. N., Darris, C. E., Chetyrkin, S., Fidler, A. L., Gallup, J.,
879 Murawala, P., Hudson, J. K., Boudko, S. P., & Hudson, B. G. (2025). Collagen IV of
880 basement membranes: I. Origin and diversification of COL4 genes enabling metazoan
881 multicellularity, evolution, and adaptation. *The Journal of Biological Chemistry*, *301*(5),
882 108496. https://doi.org/10.1016/j.jbc.2025.108496

883 Park, J. H., Jo, S. B., Lee, J.-H., Lee, H.-H., Knowles, J. C., & Kim, H.-W. (2023). Materials and
884 extracellular matrix rigidity highlighted in tissue damages and diseases: Implication for
885 biomaterials design and therapeutic targets. *Bioactive Materials*, *20*, 381–403.
886 https://doi.org/10.1016/j.bioactmat.2022.06.003

887 Parvin Nejad, S., Lecce, M., Mirani, B., Machado Siqueira, N., Mirzaei, Z., Santerre, J. P., Davies, J.
888 E., & Simmons, C. A. (2023). Serum- and xeno-free culture of human umbilical cord
889 perivascular cells for pediatric heart valve tissue engineering. *Stem Cell Research & Therapy*,
890 *14*(1), 96. https://doi.org/10.1186/s13287-023-03318-3

891 Perugini, V., & Santin, M. (2021). A Substrate-Mimicking Basement Membrane Drives the
892 Organization of Human Mesenchymal Stromal Cells and Endothelial Cells Into Perivascular
893 Niche-Like Structures. *Frontiers in Cell and Developmental Biology*, *9*, 701842.
894 https://doi.org/10.3389/fcell.2021.701842

895 Pompili, S., Latella, G., Gaudio, E., Sferra, R., & Vetuschi, A. (2021). The Charming World of the
896 Extracellular Matrix: A Dynamic and Protective Network of the Intestinal Wall. *Frontiers in*
897 *Medicine*, *8*. https://doi.org/10.3389/fmed.2021.610189

898 Ragelle, H., Naba, A., Larson, B. L., Zhou, F., Prijić, M., Whittaker, C. A., Del Rosario, A., Langer,
899 R., Hynes, R. O., & Anderson, D. G. (2017). Comprehensive proteomic characterization of

900 stem cell-derived extracellular matrices. *Biomaterials*, *128*, 147–159.
901 https://doi.org/10.1016/j.biomaterials.2017.03.008

902 Rakian, R., Block, T. J., Johnson, S. M., Marinkovic, M., Wu, J., Dai, Q., Dean, D. D., & Chen, X.-
903 D. (2015). Native extracellular matrix preserves mesenchymal stem cell "stemness" and
904 differentiation potential under serum-free culture conditions. *Stem Cell Research & Therapy*,
905 *6*, 235. https://doi.org/10.1186/s13287-015-0235-6

906 Ruiz, T. F. R., Ferrato, L. J., de Souza, L. G., Brito-Filho, G. E., Leonel, E. C. R., & Taboga, S. R.
907 (2024). The elastic system: A review of elastin-related techniques and hematoxylin-
908 eosin/phloxine applicability for normal and pathological tissue description. *Acta*
909 *Histochemica*, *126*(8), 152209. https://doi.org/10.1016/j.acthis.2024.152209

910 Sagaradze, G. D., Basalova, N. A., Efimenko, A. Y., & Tkachuk, V. A. (2020). Mesenchymal
911 Stromal Cells as Critical Contributors to Tissue Regeneration. *Frontiers in Cell and*
912 *Developmental Biology*, *8*. https://doi.org/10.3389/fcell.2020.576176

913 Sart, S., Tsai, A.-C., Li, Y., & Ma, T. (2014). Three-dimensional aggregates of mesenchymal stem
914 cells: Cellular mechanisms, biological properties, and applications. *Tissue Engineering. Part*
915 *B, Reviews*, *20*(5), 365–380. https://doi.org/10.1089/ten.TEB.2013.0537

916 Satyam, A., Kumar, P., Cigognini, D., Pandit, A., & Zeugolis, D. I. (2016). Low, but not too low,
917 oxygen tension and macromolecular crowding accelerate extracellular matrix deposition in
918 human dermal fibroblast culture. *Acta Biomaterialia*, *44*, 221–231.
919 https://doi.org/10.1016/j.actbio.2016.08.008

920 Schindelin, J., Arganda-Carreras, I., Frise, E., Kaynig, V., Longair, M., Pietzsch, T., Preibisch, S.,
921 Rueden, C., Saalfeld, S., Schmid, B., Tinevez, J.-Y., White, D. J., Hartenstein, V., Eliceiri,

922 K., Tomancak, P., & Cardona, A. (2012). Fiji: An open-source platform for biological-image
923 analysis. *Nature Methods*, *9*(7), 676–682. https://doi.org/10.1038/nmeth.2019

924 Schneider, K. H., Goldberg, B. J., Hasturk, O., Mu, X., Dötzlhofer, M., Eder, G., Theodossiou, S.,
925 Pichelkastner, L., Riess, P., Rohringer, S., Kiss, H., Teuschl-Woller, A. H., Fitzpatrick, V.,
926 Enayati, M., Podesser, B. K., Bergmeister, H., & Kaplan, D. L. (2023). Silk fibroin, gelatin,
927 and human placenta extracellular matrix-based composite hydrogels for 3D bioprinting and
928 soft tissue engineering. *Biomaterials Research*, *27*(1), 117. https://doi.org/10.1186/s40824-
929 023-00431-5

930 Sekiguchi, R., & Yamada, K. M. (2018). Basement membranes in development and disease. *Current*
931 *Topics in Developmental Biology*, *130*, 143–191. https://doi.org/10.1016/bs.ctdb.2018.02.005

932 Sharma, S., Agashe, A., Hill, J. C., Ganguly, K., Sharma, P., Richards, T. D., Huang, W.,
933 Kaczorowski, D. J., Sanchez, P. G., Kapania, R., Phillippi, J. A., & Nain, A. S. (2025).
934 Mechanical cues guide the formation and patterning of 3D spheroids in fibrous environments.
935 *PNAS Nexus*, *4*(9), pgaf263. https://doi.org/10.1093/pnasnexus/pgaf263

936 Shearier, E., Xing, Q., Qian, Z., & Zhao, F. (2016). Physiologically Low Oxygen Enhances
937 Biomolecule Production and Stemness of Mesenchymal Stem Cell Spheroids. *Tissue*
938 *Engineering. Part C, Methods*, *22*(4), 360. https://doi.org/10.1089/ten.tec.2015.0465

939 Smith, A., Huang, M., Watkins, T., Burguin, F., Baskin, J., & Garlick, J. A. (2020). De novo
940 production of human extracellular matrix supports increased throughput and cellular
941 complexity in 3D skin equivalent model. *Journal of Tissue Engineering and Regenerative*
942 *Medicine*, *14*(8), 1019–1027. https://doi.org/10.1002/term.3071

943 Solomonov, I., Kollet, O., & Sagi, I. (2025). Extracellular matrix and proteolysis: Mechanisms
944 driving irreversible changes and shaping cell behavior. *The FEBS Journal*.
945 https://doi.org/10.1111/febs.70292

946 Spoerer, T. M., Larey, A. M., Asigri, W., Daga, K. R., & Marklein, R. A. (2025). High throughput
947 morphological screening identifies chemically defined media for mesenchymal stromal cells
948 that enhances proliferation and supports maintenance of immunomodulatory function. *Stem*
949 *Cell Research & Therapy*, *16*, 125. https://doi.org/10.1186/s13287-025-04206-8

950 Tao, F., Sayo, K., Sugimoto, K., Aoki, S., & Kojima, N. (2020). Development of a tunable method to
951 generate various three-dimensional microstructures by replenishing macromolecules such as
952 extracellular matrix components and polysaccharides. *Scientific Reports*, *10*, 6567.
953 https://doi.org/10.1038/s41598-020-63621-4

954 Trębacz, H., & Barzycka, A. (2023). Mechanical Properties and Functions of Elastin: An Overview.
955 *Biomolecules*, *13*(3), 574. https://doi.org/10.3390/biom13030574

956 Tsai, A.-C., Liu, Y., Yuan, X., & Ma, T. (2015). Compaction, Fusion, and Functional Activation of
957 Three-Dimensional Human Mesenchymal Stem Cell Aggregate. *Tissue Engineering. Part A*,
958 *21*(9–10), 1705–1719. https://doi.org/10.1089/ten.tea.2014.0314

959 Tuftee, C., Alsberg, E., Ozbolat, I. T., & Rizwan, M. (2024). Emerging granular hydrogel bioinks to
960 improve biological function in bioprinted constructs. *Trends in Biotechnology*, *42*(3), 339–
961 352. https://doi.org/10.1016/j.tibtech.2023.09.007

962 Turlier, H., & Maître, J.-L. (2015). Mechanics of tissue compaction. *Seminars in Cell &*
963 *Developmental Biology*, *47–48*, 110–117. https://doi.org/10.1016/j.semcdb.2015.08.001

964 van der Net, A., Rahman, Z., Bordoloi, A. D., Muntz, I., ten Dijke, P., Boukany, P. E., &
965 Koenderink, G. H. (2024). EMT-related cell-matrix interactions are linked to states of cell
966 unjamming in cancer spheroid invasion. *iScience*, *27*(12), 111424.
967 https://doi.org/10.1016/j.isci.2024.111424

968 Walker, C. J., Crocini, C., Ramirez, D., Killaars, A. R., Grim, J. C., Aguado, B. A., Clark, K., Allen,
969 M. A., Dowell, R. D., Leinwand, L. A., & Anseth, K. S. (2021). Nuclear mechanosensing
970 drives chromatin remodelling in persistently activated fibroblasts. *Nature Biomedical*
971 *Engineering*, *5*(12), 1485–1499. https://doi.org/10.1038/s41551-021-00709-w

972 Weber, T., Bajramovic, J., & Oredsson, S. (2024). Preparation of a universally usable, animal
973 product free, defined medium for 2D and 3D culturing of normal and cancer cells. *MethodsX*,
974 *12*, 102592. https://doi.org/10.1016/j.mex.2024.102592

975 Wiese, D. M., & Braid, L. R. (2020). Transcriptome profiles acquired during cell expansion and
976 licensing validate mesenchymal stromal cell lineage genes. *Stem Cell Research and Therapy*,
977 *11*(1), 1–7. https://doi.org/10.1186/S13287-020-01873-7/FIGURES/3

978 Wiese, D. M., Ruttan, C. C., Wood, C. A., Ford, B. N., & Braid, L. R. (2019). Accumulating
979 Transcriptome Drift Precedes Cell Aging in Human Umbilical Cord-Derived Mesenchymal
980 Stromal Cells Serially Cultured to Replicative Senescence. *STEM CELLS Translational*
981 *Medicine*, *8*(9), 945–958. https://doi.org/10.1002/SCTM.18-0246

982 Wiese, D. M., Wood, C. A., Ford, B. N., & Braid, L. R. (2022). Cytokine Activation Reveals Tissue-
983 Imprinted Gene Profiles of Mesenchymal Stromal Cells. *Frontiers in Immunology*, *13*.
984 https://www.frontiersin.org/articles/10.3389/fimmu.2022.917790

985 Xu, J., Lian, W., Chen, J., Li, W., Li, L., & Huang, Z. (2020). Chemical-defined medium supporting
986 the expansion of human mesenchymal stem cells. *Stem Cell Research & Therapy*, *11*, 125.
987 https://doi.org/10.1186/s13287-020-01641-7

988 Yin, S., Wu, H., Huang, Y., Lu, C., Cui, J., Li, Y., Xue, B., Wu, J., Jiang, C., Gu, X., Wang, W., &
989 Cao, Y. (2024). Structurally and mechanically tuned macroporous hydrogels for scalable
990 mesenchymal stem cell–extracellular matrix spheroid production. *Proceedings of the National*
991 *Academy of Sciences*, *121*(28), e2404210121. https://doi.org/10.1073/pnas.2404210121

992 Yokomine, S., Makino, T., Nagao, E., & Nakazawa, K. (2025). Floating or adherent hepatocyte
993 spheroid cultures using microwell chips with polyethylene glycol or polyimide surfaces.
994 *Biomedical Materials*, *20*(3), 035009. https://doi.org/10.1088/1748-605X/adc17d

995 Yu, L. T., Kreutzberger, M. A. B., Bui, T. H., Hancu, M. C., Farsheed, A. C., Egelman, E. H., &
996 Hartgerink, J. D. (2024). Exploration of the hierarchical assembly space of collagen-like
997 peptides beyond the triple helix. *Nature Communications*, *15*(1), 10385.
998 https://doi.org/10.1038/s41467-024-54560-z

999 Yurchenco, P. D. (2011). Basement Membranes: Cell Scaffoldings and Signaling Platforms. *Cold*
1000 *Spring Harbor Perspectives in Biology*, *3*(2), a004911.
1001 https://doi.org/10.1101/cshperspect.a004911

1002 Zhang, X., Battiston, K. G., Labow, R. S., Simmons, C. A., & Santerre, J. P. (2017). Generating
1003 favorable growth factor and protease release profiles to enable extracellular matrix
1004 accumulation within an *in vitro* tissue engineering environment. *Acta Biomaterialia*, *54*, 81–
1005 94. https://doi.org/10.1016/j.actbio.2017.02.041

1006 Zhang, Y., Feng, Y., Shao, Q., Jiang, Z., & Yang, G. (2023). Rapid formation of 3D: Decellularized
1007 extracellular matrix spheroids for enhancing bone formation. *Journal of Biomedical Materials*
1008 *Research. Part A*, *111*(3), 378–388. https://doi.org/10.1002/jbm.a.37471

1009 Zhao, W., Zhu, J., Hang, J., & Zeng, W. (2022). Biomaterials to promote vascularization in tissue
1010 engineering organs and ischemic fibrotic diseases. *MedComm – Biomaterials and*
1011 *Applications*, *1*(1), e16. https://doi.org/10.1002/mba2.16

1012 Zhou, Y., Chen, H., Li, H., & Wu, Y. (2017). 3D culture increases pluripotent gene expression in
1013 mesenchymal stem cells through relaxation of cytoskeleton tension. *Journal of Cellular and*
1014 *Molecular Medicine*, *21*(6), 1073–1084. https://doi.org/10.1111/jcmm.12946

1015

1016